3.06 Tidal Flat Morphodynamics: A Synthesis

CT Friedrichs, Virginia Institute of Marine Science, Gloucester Point, VA, USA

3.06.1	**Introduction**	138
3.06.1.1	Occurrence and Definition of Tidal Flats	138
3.06.1.2	Definition of Morphodynamics and Concept of Dynamic Equilibrium	138
3.06.1.3	Tidal Asymmetry: Importance and Basic Types	139
3.06.2	**Net Transport due to Spatial (Lagrangian) Asymmetries**	140
3.06.2.1	Lagrangian Asymmetry, Concentration Gradients, and Lag-Induced Dispersion	140
3.06.2.2	Nature of Tide- and Wave-Induced Spatial Energy Gradients	141
3.06.2.3	Observations of Net Transport on Tidal Flats due to Waves versus Tides	142
3.06.2.4	Observations of Net Transport on Tidal Flats due to Other Sediment Sources or Sinks	144
3.06.3	**Net Transport due to Eulerian Asymmetries**	146
3.06.3.1	Definitions and Types of Eulerian Asymmetry	146
3.06.3.2	Eulerian Velocity Asymmetries Induced by Continuity Alone	147
3.06.3.3	Eulerian Asymmetries Induced by Momentum plus Continuity	148
3.06.3.4	Observations of Eulerian Asymmetries and Resulting Sediment Transport	149
3.06.4	**Theoretical Equilibria in Response to Tides, Waves, and Sediment Supply**	150
3.06.4.1	Convex-Up Profile in Response to Uniform Maximum Tidal Velocity	150
3.06.4.2	Equilibrium Shape in Response to Tidal Range and Sediment Supply	151
3.06.4.3	Equilibrium in Response to Persistent Tidal Asymmetries	152
3.06.4.4	Concave-Up Equilibrium in Response to Waves	154
3.06.4.5	A Solution to Predict Tidal Flat Width in Response to Waves	154
3.06.4.6	Theoretical Predictions of Equilibrium Slope under Wave Dominance	155
3.06.4.7	Predictions of Equilibria in the Presence of Waves, Tides, and Sediment Supply	155
3.06.5	**Observed Morphology in Response to Tides, Waves, and Sediment Supply**	156
3.06.5.1	Profile Convexity/Concavity as a Function of Tidal Range and Wave Exposure	156
3.06.5.2	Profile Width and Slope as a Function of Tidal Range and Wave Exposure	157
3.06.5.3	Depositional versus Erosional Flats	159
3.06.5.4	Combined Effects of Tides, Waves and Recent Erosion or Deposition	160
3.06.6	**Extreme Timescales of Change: From Sea Level to Grain Size Patterns**	162
3.06.6.1	Timescales of Change	162
3.06.6.2	Mean Grain-Size Patterns	163
3.06.6.3	Time-Varying Grain-Size Patterns	164
3.06.7	**Summary and Conclusions**	165
References		169

Abstract

The study of the morphology and evolution of tidal flats is particularly well suited in the context of morphodynamics in that characteristics such as profile shape, bed slope, and grain size clearly and systematically vary as a function of sediment supply and wave and tidal forcing, and the nature of wave- and tide-induced velocities across tidal flats is, in turn, a direct function of the tidal flat morphology itself. When averaged over annual or longer timescales, tidal flat morphology typically approximates a dynamic equilibrium with external forcing. Over seasonal and shorter timescales, spatial asymmetries in the hydrodynamic energy associated with temporally alternating tide- and wave-dominance drive sediment landward and seaward, respectively. For flats exhibiting minimal spatial gradients in energy, net sediment transport can still occur in response to local, time-dependent asymmetries associated with finite depth and intertidal storage effects; negative feedback on the scale of entire tidal embayments may favor minimization of these local asymmetries. Assuming that morphological equilibrium is likewise associated with the minimization of spatial asymmetries in energy, dominance by tides results in a convex-up tidal flat profile, whereas dominance by waves results in a concave-up profile. These extremes lead to analytical solutions for tidal flat width, slope, and degree of curvature as a function of tidal range, wave height, and the critical velocity for profile stability. Although a tide- or wave-dominated static equilibrium theoretically exists at each of these extremes, natural tidal flats over annual timescales are better approximated by a dynamic equilibrium somewhere between these two asymptotes. Observations and models indicate that, within this range of morphologies, convex-up profiles are further favored by increased sediment supply, increased bioaggregation/adhesion, and external forcing by faster-rising tides; concave-up profiles are further favored by decreased sediment supply, increased bioturbation, and external forcing by faster-falling tides. Processes/properties associated with evolution toward a convex (vs. concave) profile include shoreward (vs. seaward) sediment transport, net deposition (vs. erosion), decreased (vs. increased) grain size, and a form that progrades seaward

(vs. retreating landward). Because surficial grain size responds to energy gradients much more quickly than overall morphology can adjust, the common presence of tides without strong waves (alternating with much shorter periods of intense waves) leads to landward fining of surficial grain size most of the time.

3.06.1 Introduction

3.06.1.1 Occurrence and Definition of Tidal Flats

Tidal flats are common in sediment-rich environments where the tidal range is large relative to typical wave height. Although larger tidal ranges are particularly conducive to flat formation, tidal flats can also occur where the mean range is less than a meter, as long as mean wave heights are several times smaller (Hayes, 1979). As tidal range decreases in the absence of waves, however, mangroves or tidal marsh is likely to occupy an increasingly large fraction of the intertidal surface area (Amos, 1995). This chapter focuses on large-scale patterns extending across tidal flats, including patterns of bed slope and grain size. This chapter does not focus in detail on the morphology of either tidal flat bedforms or the channels that commonly cross tidal flats.

Here, we define tidal flats as low bed slope environments, consisting of sediments in the absence of abundant tidal marsh or mangroves, and which are exposed subaerially between lowest and highest astronomical tide (cf. Amos, 1995). Like Amos (1995), we also recognize that this definition does not always correspond to sharp morphological or sedimentological boundaries. In many cases, there exists a gradual morphological transition extending beyond low tide, in that similar tide- and wave-driven processes often continue to move sediment sub-tidally, such that the lower parts of some tidal flats may behave much like mudbanks (Mehta, 2002). A gradual transition may also occur above high tide, in that supratidal storm surges or river floods may blur the upper boundary for cases where vegetation is not present. In addition, the low bed slope criterion, which distinguishes tidal flats from beaches or channel flanks, is not exact, nor is the density of plants needed to precisely define the transition to a marsh or mangrove. Nonetheless, the above description provides a reasonable working definition.

Several review articles have appeared over the last few decades focusing in large part on the sedimentology and/or geomorphology of tidal flats (Pethick, 1984, 1996; Klein, 1985; Amos, 1995; Dyer, 1998; Dyer et al., 2000; Gao, 2009), with Amos (1995) and Pethick (1996) concentrating the most on morphodynamic issues. Although both of these morphodynamic studies are highly instructive, the Amos (1995) review focuses mainly on sand-rich tidal flats fringing large coastal embayments (such as the Wash and the Bay of Fundy; e.g., **Figure 1(a)**), while the Pethick (1996) review focuses mainly on more sheltered, muddy tidal flats within estuaries (such as the Humber and the Dutch Wadden Sea; e.g., **Figure 1(b)**). By contrast, this chapter attempts to (1) synthesize the morphodynamics of tidal flats of all grain sizes along both sheltered and open coasts and (2) build on the insights of Amos (1995) and Pethick (1996) by incorporating additional morphodynamic findings reported over subsequent years.

3.06.1.2 Definition of Morphodynamics and Concept of Dynamic Equilibrium

Morphodynamics is the process by which morphology affects hydrodynamics in such a way as to influence the further

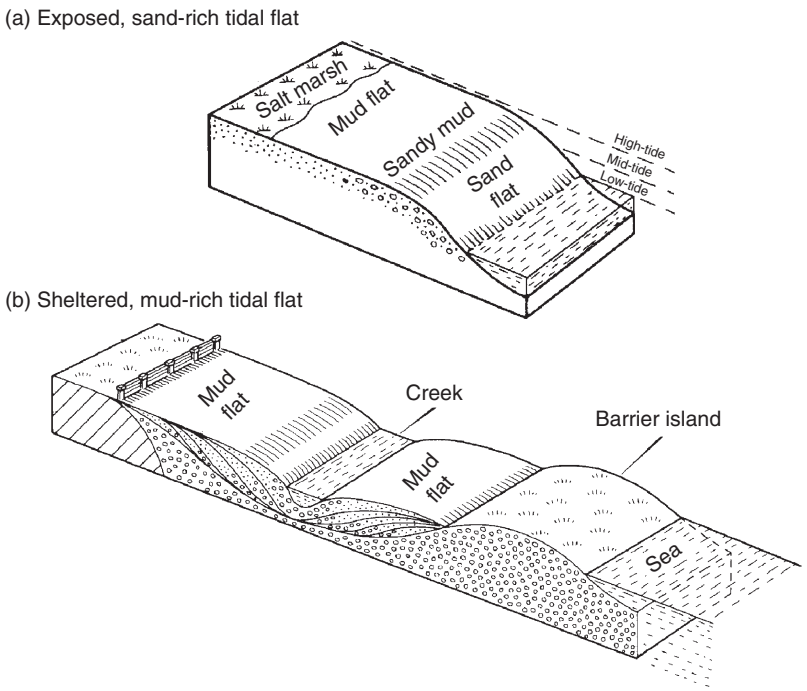

Figure 1 Relationships between tidal flat morphology and sediment variation as found in (a) an exposed sand-rich coastal flat such as the Wash, UK, and (b) a mud-rich sheltered flat such as the Dutch Wadden Sea. Both types of tidal flats are usually characterized by an overall landward decrease in grain size, although sheltered flats tend to be exposed to lower energy overall and are thus generally finer grained. Modified from Pethick, J.S., 1984. An Introduction to Coastal Geomorphology. Arnold, London, 272 pp.

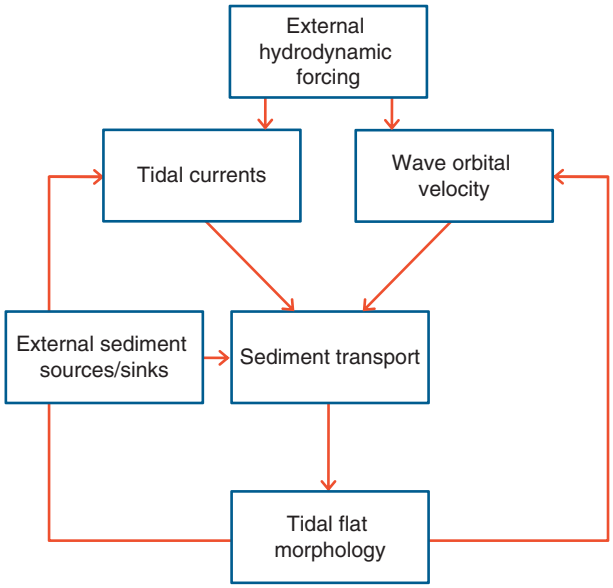

Figure 2 Simplified morphodynamic components influencing tidal flat evolution. Morphodynamics is the process by which morphology affects hydrodynamics in such a way as to influence the further evolution of the morphology itself. Possibly significant components, not illustrated in this schematic, include grain size variation, biological activity, antecedent geology, anthropogenic impact, and long-term variation in relative sea level.

evolution of the morphology itself (e.g., Wright, 1995; Friedrichs and Perry, 2001; de Swart and Zimmerman, 2009; **Figure 2**). The study of the morphology and evolution of tidal flats is particularly well suited in the context of morphodynamics, in that characteristics such as profile shape, bed slope, and grain size clearly and systematically vary as a function of sediment supply and wave and tidal forcing, and the nature of wave- and tide-induced velocities across tidal flats is, in turn, a direct function of the tidal flat morphology itself (Amos, 1995; Pethick, 1996).

Here, we somewhat loosely define an equilibrium tidal flat profile as one with a shape that remains more or less constant over some characteristic period of natural forcing. This definition is purposely qualitative in order to encompass the type of variability found in nature, where even the most stable morphologies are rarely completely static (Woodroffe, 2002). Along the spectrum of natural equilibria, a relatively simple but extreme case is that for which there is never significant instantaneous sediment motion. This criterion is approximately satisfied if the maximum current speed at equilibrium is everywhere equal to the critical erosion velocity (cf. Friedrichs, 1995). However, more commonly we define an at least temporary dynamic equilibrium to hold when net transport nearly vanishes over some characteristic time period during which instantaneous transport is not necessarily negligible, such as over an entire 12- or 24-h tidal cycle, a spring–neap cycle, an annual cycle, or a storm plus recovery cycle.

When considering even longer periods, typically of the order of decades or more, the shape of a tidal flat profile may remain nearly constant while expanding seaward or contracting landward as sediment is imported to or exported from the system (Pritchard and Hogg, 2003). Over still longer timescales, a tidal flat might accrete vertically in response to a rise in mean sea level. If the profile's long-term topography remains more or less constant relative to the local low and high water over the course of a horizontal or vertical translation, we will still define the profile shape as being near a dynamic equilibrium (cf. Cowell and Thom, 1994). However, we specifically do not require the external forcing to be constant in order to approach what is defined here as a near-equilibrium form. In fact, natural tidal flats, which commonly evolve toward dynamic equilibria, most typically respond over the course of a given year to highly unsteady mixes of off- and onshore transport forced by ever-changing combinations of waves and tides.

The concept of a dynamic equilibrium is a central point of this chapter. When considered as an average over a typical annual cycle, this chapter proposes that most tidal flats are characterized by predictable morphologies that are in an approximate dynamic equilibrium with their local climate of waves, tides, and sediment sources and sinks. Although additional external constraints such as immobile antecedent geology and human engineering must often be considered, relatively subtle aspects of tidal flat morphology, including the degree of profile convexity or concavity and temporal variations in the surficial transition from sand to mud, can still be understood in terms of tidal advection of cross-shore gradients in suspended sediment concentration induced, in turn, by gradients in hydrodynamic energy and sediment/seabed properties.

3.06.1.3 Tidal Asymmetry: Importance and Basic Types

In order to identify the conditions of morphodynamic equilibrium (or disequilibrium) associated with tidal flats, we must first understand the processes that lead to net sediment transport over a tidal cycle or longer (cf. de Swart and Zimmerman, 2009). As tidal processes are, by definition, periodic, there must be some sort of spatial or temporal asymmetry present for tidally varying processes to induce net transport. If the

conditions to which the studied sediment were subjected over a flood and ebb were exactly the same, no net transport would occur.

To aid in conceptual understanding, it is useful to divide the asymmetries which drive net transport across tidal flats into two basic types: local (Eulerian) asymmetries and spatial (Lagrangian) asymmetries (e.g., Ridderinkhof, 1997; Pritchard, 2005). Note that for the purposes of defining local versus spatial asymmetry, the focus here is more on the asymmetry of the environmental forcing and/or boundary conditions, rather than the asymmetry of the resulting concentration field. Despite the convenience of these two categories, it should be kept in mind that these two types of asymmetries typically occur simultaneously, although their relative importance will vary as a function of sediment type, hydrodynamic energy, sediment supply, local tidal flat shape, and surrounding coastal morphology.

3.06.2 Net Transport due to Spatial (Lagrangian) Asymmetries

3.06.2.1 Lagrangian Asymmetry, Concentration Gradients, and Lag-Induced Dispersion

Net sediment transport by Lagrangian asymmetry is a sort of tidal dispersion in that it drives suspended sediment from areas of higher concentration toward areas of lower concentration and can result in net transport even if local (i.e., Eulerian) variations in velocity, stress, turbulence, and water depth are identical during the flood and ebb tidal cycles. Classically, Lagrangian asymmetries in tidal flat systems are largely driven by spatial variations in total hydrodynamic energy working in concert with time lags in the relationship between instantaneous bed stress and depth-integrated suspended sediment concentration (Ridderinkhof, 1998; Pritchard, 2005). As the tide moves sediment-laden water from areas of higher stress toward areas of lower stress, it takes a finite period of time for the suspended sediment to respond to reduced turbulence and settle to the bed. Thus, there is temporarily a surplus of suspended sediment relative to the instantaneous bed stress (**Figure 3**(**a**)). When the tide moves the water back toward higher stress areas, sediment concentration lags behind the now increasing stress – this time because it takes a finite period for the sediment to be resuspended back up from the bed. As a consequence, there is now a deficit of suspended sediment relative to the instantaneous bed stress (**Figure 3**(**b**)) and water parcels therefore contain less sediment when they return to high-energy regions than when they leave, thus causing a net flux of sediment toward areas of lower energy.

Spatial variations in the local water depths over which sediment-laden water parcels traverse can reinforce or counteract the above pattern. If the period of low velocities around slack water is short, a smaller fraction of the total suspended mass will have time to settle out in deeper areas. In shallower areas, a larger fraction of the total suspended mass will have time to settle. This trend favors net deposition in shallower areas (de Swart and Zimmerman, 2009). Over very low energy intertidal areas, however, the overall duration of submersion can counteract the above effect. Over a full tidal cycle, lower elevation tidal flats are submerged longer than higher elevation flats; therefore, if energy is almost always low, as might be the case across relatively small, sheltered flats, there will be more time for very fine sediment to settle in deeper intertidal areas. This hydroperiod effect has been especially well documented with regard to topographic control of fine-sediment deposition patterns on tidal marshes (Reed, 1990; Friedrichs and Perry, 2001).

In the context of following an individual sediment particle over one or more tidal excursions, a number of authors have

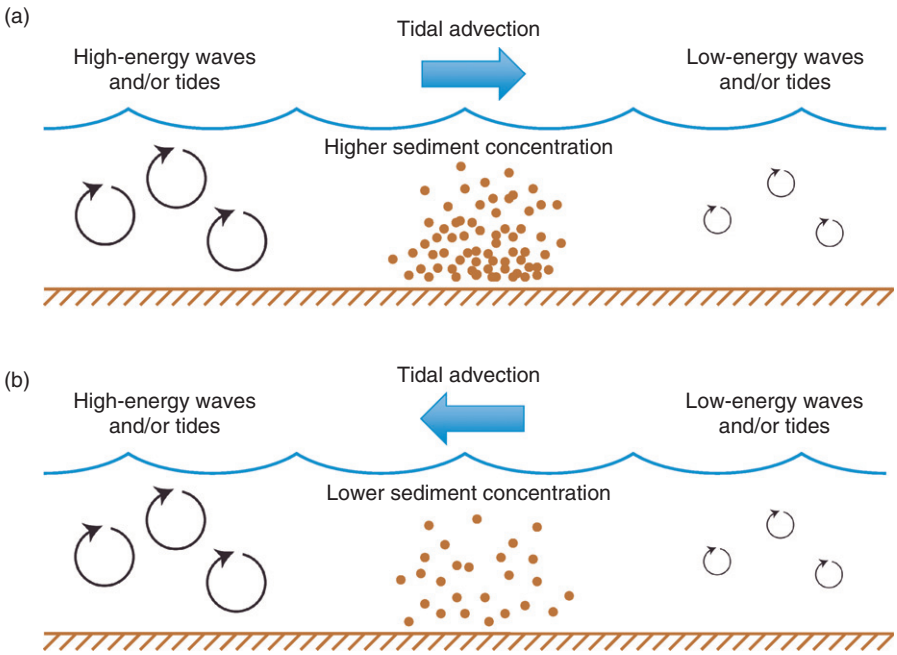

Figure 3 Because suspended sediment concentration lags behind instantaneous bottom stress (and assuming uniform bed conditions), (a) tidal currents moving away from areas of higher energy will carry more sediment than (b) tidal currents moving away from areas of lower energy. As a result, there is a net flux of sediment advected by the tide toward areas of lower energy.

termed Lagrangian lag-based net transport mechanisms associated with deposition and erosion as 'settling lag' and 'scour lag', respectively (Van Straaten and Kuenen, 1958; Postma, 1961; Nichols and Biggs, 1985; Pritchard and Hogg, 2003). However, representation of the sediment field as a single particle makes it more difficult to estimate the fraction of the total sediment field that is likely to settle at a given time. Tracking a single representative particle may also erroneously suggest the prevalence of net transport against an opposing concentration gradient (Nichols and Biggs, 1985). In the context of an infinite number of particles plus appropriate random perturbations, representation by individual particles becomes equivalent to representation by a concentration field. Nonetheless, in this chapter we emphasize the concentration field viewpoint, which implicitly incorporates stochastic variability within continuum dynamics (Pritchard and Hogg, 2003).

Besides a lag in the response of depth-integrated concentration to local hydrodynamics, net transport of sediment concentration by purely Lagrangian asymmetries requires: (1) horizontal gradients in concentration and (2) periodic water parcel excursions. Spatial gradients in sediment concentration can be driven by gradients in tidal energy, wave energy, depth-dependent settling time, sediment supply, and/or bed properties. The ramifications of spatial gradients in energy associated with tides and waves are the main focus of this chapter. However, any cause of spatial asymmetries in sediment concentration can lead to lag-driven net transport (**Figure 4**), including impacts of local runoff or riverine input, sorted bed grain sizes, spatially varying bed consolidation (including desiccation), bioturbation, bioadhesion, particle aggregation, and/or trapping in an adjacent marsh.

Periodic water parcel movement and sediment advection on tidal flats is primarily in response to the dominant tidal excursion. However, quasi-periodic horizontal circulations of all sizes, including eddies, wind-wave orbital motions, and horizontal turbulence contribute to dispersing suspended sediment down its concentration gradient via analogous processes (cf. de Swart and Zimmerman, 2009). In this respect, transport induced by Lagrangian asymmetries also incorporates smaller-scale periodic, chaotic, or turbulent dispersion.

3.06.2.2 Nature of Tide- and Wave-Induced Spatial Energy Gradients

In order to assess likely trends in hydrodynamic energy across tidal flats (and their resulting potential for producing horizontal concentration gradients), it is useful to consider simple cases for the spatial distribution of tide- and wave-induced velocities, respectively, across linearly sloping flats **Figure 5(a)**). Across-shore, depth-averaged tidal velocity (U_T) is approximated here based on the continuity equation alone, and our estimates of wave orbital velocity amplitude (U_W) assume linear, unbroken, shallow-water waves (cf, Friedrichs and Aubrey, 1996). For the calculations given below, tidal elevation (η) is assumed to be sinusoidal in time and uniform in space, bathymetric contours are straight and shore-parallel, and wave height is kept fixed in both time and space. (Note that the constant wave height assumption neglects wave shoaling, frictional dissipation, and depth-limited breaking.) This approach then gives (for $x \le x_f$)

$$U_T(x,t) = [(x_f(t) - x)/h(x,t)]\, \mathrm{d}(\eta(t))/\mathrm{d}t \qquad [1a]$$

$$U_W(x,t) = (1/2)\,(H/h(x,t))\,(gh(x,t))^{1/2} \qquad [1b]$$

$$h(x,t) = \eta(t) - Z(x) \qquad [1c]$$

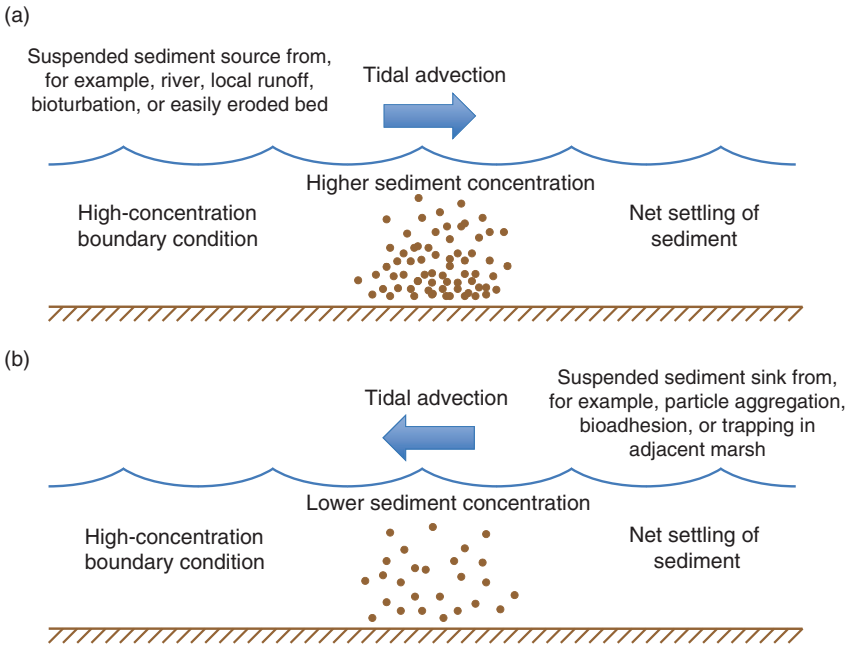

Figure 4 Other causes of spatial asymmetries in sediment concentration besides bed stress over the flat itself can lead to lag-driven net transport. For example, (a) tidal currents moving away from a suspended sediment source in an adjacent river, from local runoff or from an easily eroded bed region are likely to carry more sediment than (b) tidal currents moving away from a region of bed desiccation, strong bioadhesion, or trapping in an adjacent marsh.

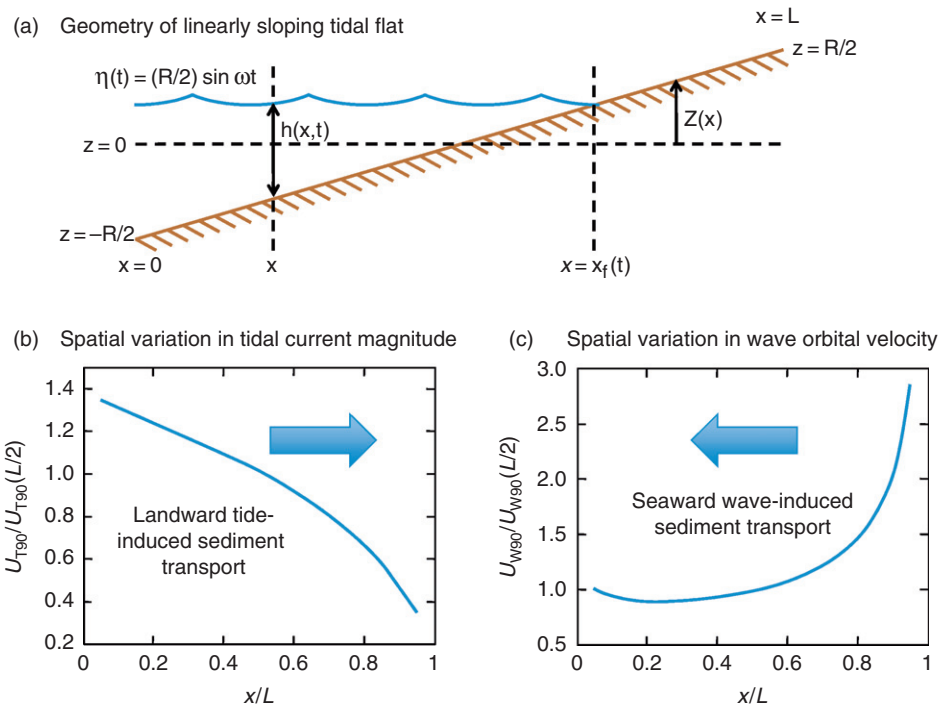

Figure 5 (a) Side view of a linearly sloping flat: x is landward distance across a flat of width L, $\eta(t)$ is tidal elevation, R is tidal range, $h(x,t)$ is local depth, x_f is the position of the tidal front, and $Z(x)$ is the elevation of the profile. Across-flat variation in the 90th percentile of (b) tidal current velocity (U_{T90}) and (c) wave orbital velocity (U_{W90}) are calculated from eqn [1]. Tidal and wave energy gradients favor landward and seaward net sediment transport, respectively.

Figures 5(**b**) and 5(**c**) display the spatial distribution of the 90th percentile of velocity based on eqns [1a]–[1c] for tidal currents (U_{T90}) and wave orbital velocities (U_{W90}) for times when each location across the linearly sloping flat is submerged. The use of U_{90} accounts for both the characteristic magnitude of energetic velocities as well as the fraction of time that velocities are large. In the past, U_{90} has been found by others to be a useful scale for evaluating coastal morphology (e.g., Friedrichs and Wright, 2004). In this case, U_{90} also avoids the complications introduced by the undefined wave orbital velocity at the zero-depth tidal front (x_f). Finally, normalizing the results relative to U_{90} at a point half-way across the flat highlights spatial trends independent of the other parameters (where R is the tidal range, H the wave height, L the tidal flat width, ω the tidal radian frequency, and g the gravitational acceleration).

Based on the expected distribution of tide- and wave-induced velocities (Figures 5(**b**) and 5(**c**)), it is likely that energy-driven Lagrangian asymmetries across a linearly sloping tidal flat will favor (1) landward and (2) seaward net transport of suspended sediment in the presence of (1) sinusoidally forced tides and (2) nondissipative waves, respectively. For both cases, the spatial gradient in U_{90} is strongest across the upper flat where submergence occurs only around high water. Approaching the high-water line, a slower change in η causes $U_T \sim d\eta/dt$ to rapidly decrease across a linearly sloping tidal flat. Conversely, for waves, smaller depths near the high-water line cause $U_W \sim H/h$ to increase rapidly, and a longer period of attack around high water further accentuates U_{W90}. A second, smaller increase in U_{W90} is also predicted near the low tide line because an extended period of small h also occurs there.

3.06.2.3 Observations of Net Transport on Tidal Flats due to Waves versus Tides

Observations on tidal flats of spatial gradients in suspended sediment concentration, of the direction of net sediment flux, and of bed change as a function of tidal versus wave energy all support the trends in net transport predicted by Figures 5(**b**) and 5(**c**). For example, Ridderinkhof et al. (2000) observed relative concentrations of suspended sediment in a tidal channel and on a neighboring flat in the Ems–Dollard system in the Netherlands to vary systematically as a function of wind speed (Figure 6). When winds were weak, sediment concentration was higher in the channel because tidal velocities were greater there than on the tidal flat. When winds approached 10 m s^{-1}, however, the sediment concentration gradient tended to reverse because locally generated waves produced higher bed stresses on the tidal flats. Similarly, Janssen-Stelder (2000) found that the tidally averaged flux of suspended sediment across tidal flats in the Dutch Wadden Sea was landward in the absence of waves. But, as wave height grew, the tidally averaged flux of suspended sediment became directed more strongly offshore (Figure 7(**a**)). Allen and Duffy (1998) observed accretion to occur on a suite of tidal mudflats along the Severn Estuary, UK, during months with low wave power. However, as wave power increased, the monthly change in mudflat elevation became increasingly negative (Figure 7(**b**)).

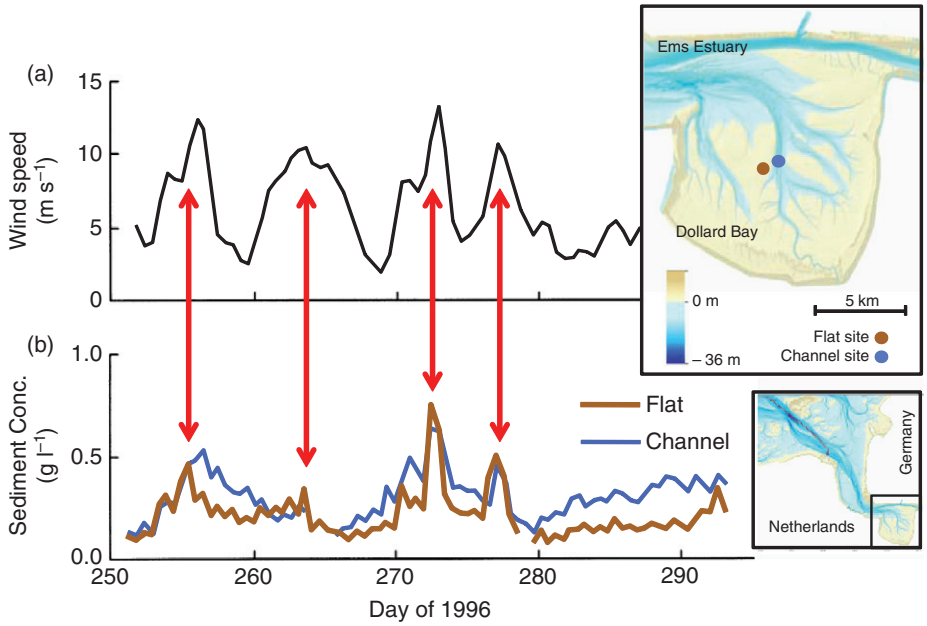

Figure 6 (a) Wind speed and (b) tidally averaged suspended sediment concentration in a tidal channel and over a neighboring tidal flat in the Ems–Dollard Estuary, The Netherlands, during August and September 1996. When winds are weak, tidal velocity in the channel favors higher concentration; however, when winds are strong, waves over the flats favor higher concentration. Modified from Ridderinkhof, H., van der Ham, R., van der Lee, W., 2000. Temporal variations in concentration and transport of suspended sediment in a channel-flat system in the Ems–Dollard estuary. Continental Shelf Research 20, 1479–1493; inset modified from Hartsuiker, G., Grasmeijer, B., van Banning, G., 2009. 3D fine sediment modeling in the Ems estuary. Estuarine Functioning and 'Muddy Waters', Estuarine and Coastal Sciences Association, Emden, Germany, 9–10 December.

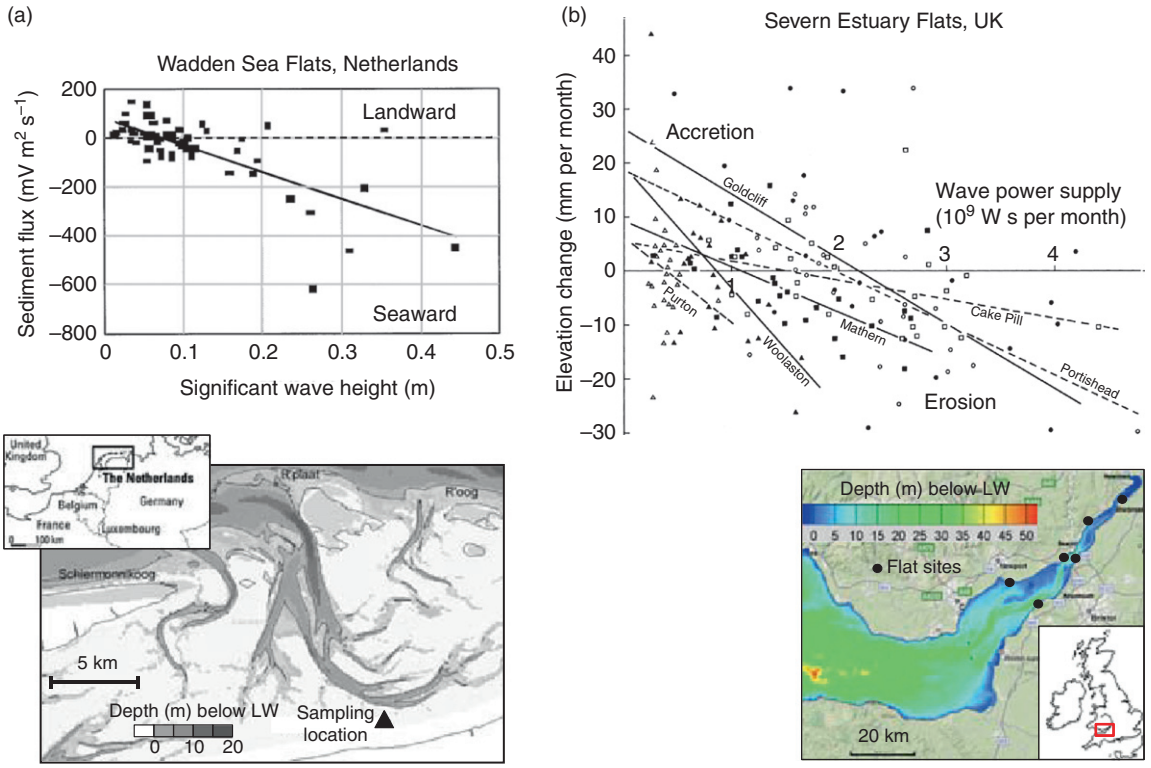

Figure 7 Net sediment flux (with positive values for landward sediment transport or accretion) as function of wave height or power: (a) average semi-diurnal sediment flux (with mV from sediment-induced optical backscatter) versus high water significant wave height for October 1998 on the Groningen tidal flat, Dutch Wadden Sea.; (b) monthly elevation change versus monthly wave power supplied to Severn Estuary tidal flats, UK, around high water between June 1991 and June 1993. In each case, tides alone result in onshore transport/accretion, whereas offshore transport/erosion increases with stronger waves. (a) Modified from Janssen-Stelder, B., 2000. The effect of different hydrodynamic conditions on the morphodynamics of a tidal mudflat in the Dutch Wadden Sea. Continental Shelf Research 20, 1461–1478. (b) Modified from Allen, J.R.L., Duffy, M.J., 1998. Medium-term sedimentation on high intertidal mudflats and salt marshes in the Severn estuary, SW Britain: the role of wind and tide. Marine Geology 150, 1–27; inset modified from Xia, J., Falconer, R.A., Lin, B., 2010. Hydrodynamic impact of a tidal barrage in the Severn estuary. Renewable Energy 35, 1455–1468.

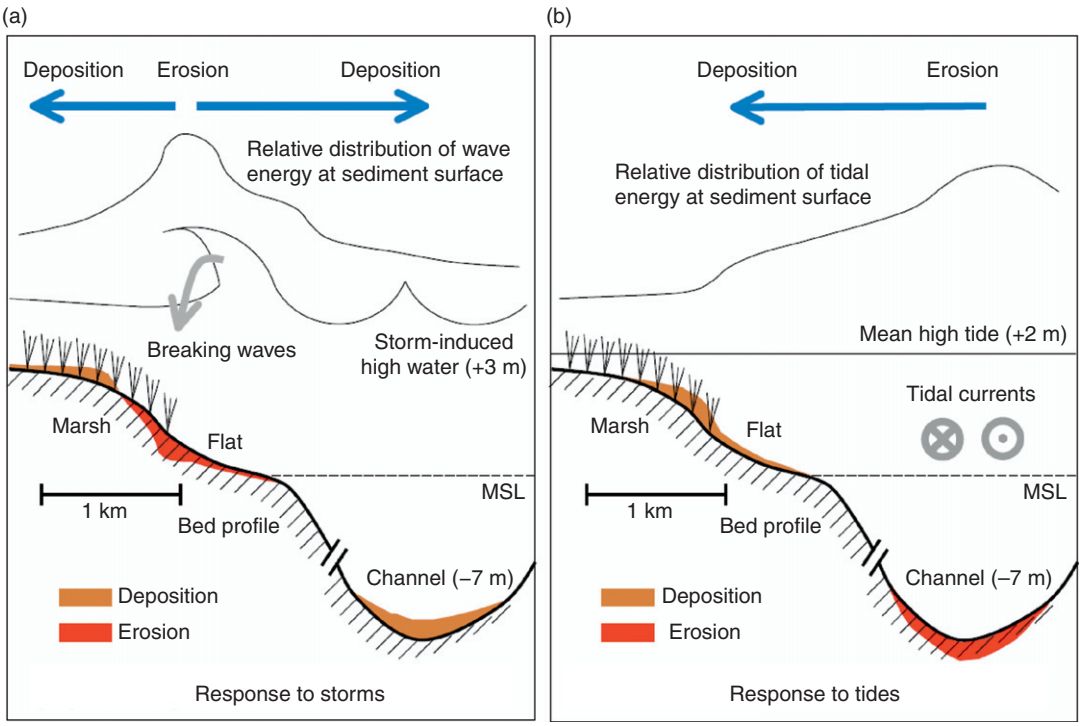

Figure 8 Conceptual model for the morphodynamic response of the coastline of the outer Yangtze River mouth to (a) major storms and (b) typical spring tides. In each case, sediment moves away from areas of higher energy and toward areas of lower energy. (b) Modified from Yang, S.L., Friedrichs, C.T., Shi, Z., Ding, P.X., Zhu, J., Zhao, Q.Y., 2003. Morphological response of tidal marshes, flats and channels of the outer Yangtze River mouth to a major storm. Estuaries 26, 1416–1425.

Yang et al. (2003) developed a conceptual model for evolution of tidal flats at the mouth of the Yangtze River, China, where a landward increase in wave energy felt at the seabed drives sediment seaward during storms (**Figure 8(a)**), and a landward decrease in tidal energy drives sediment landward during calm conditions (**Figure 8(b)**). Several other tidal flat studies have also documented a tendency for tidal flat erosion during periods of high waves alternating with tidal flat deposition in the presence of mainly tidal currents (e.g., Wells et al., 1990; Lee et al., 2004; Yang et al., 2008). Note that during storms, wave energy eventually decreases shoreward of the Yangtze flats (**Figure 8(a)**), such that sediment is driven onto the neighboring marsh. In contrast to tidal flats, wave dissipation by marsh grass often causes tidal marshes to vertically accrete in response to storms (Friedrichs and Perry, 2001). In analogy with marshes, the presence of fluid mud offshore of open-coast tidal flats can potentially dampen wave energy to the extent that energy at the seabed decreases toward shore, favoring shoreward sediment dispersion (Wells and Kemp, 1986; Allison et al., 1995).

3.06.2.4 Observations of Net Transport on Tidal Flats due to Other Sediment Sources or Sinks

A common case of a supply-driven gradient contributing to tidal flat deposition is the boundary condition of high sediment concentrations from a tidal river driving suspended sediment onto nearby flats (e.g., Allison et al., 1995; Deloffre et al., 2005; Bearman et al., 2010b). Along the macrotidal freshwater section of the Seine, for example, tidal flats accrete during the winter when riverine flow and sediment concentrations are especially high, exceeding concentrations present in the adjacent downstream estuary (Deloffre et al., 2005; **Figure 9**). Under these conditions, sediment is moved by dispersion from the higher turbidity river channel out onto the adjacent tidal flats (cf. **Figure 4**), with the extended duration of tidal flat submersion associated with higher river levels further favoring deposition. During the remainder of the year, tidal dispersion drives mud resuspended by relatively high stresses on the flats back toward the much lower concentration water found in the river channel during periods of weaker discharge.

Another site at which fluctuating riverine sediment supply has been identified to be a main cause of net tidal flat deposition or erosion is San Francisco Bay. Bearman et al. (2010b) correlated elevation changes on tidal flats in South San Francisco Bay between the 1890s and 2005 to fluctuations in supply from neighboring rivers. Long-term erosion on flats in the north end of the study area was correlated to a decrease in sediment discharge from the Sacramento and San Joaquin rivers to the north, while long-term stability on flats in the south end was correlated to steadier discharge from the San Jose River to the south.

Spatial gradients in suspended sediment concentration across tidal flats can also arise from gradients in the critical stress necessary for sediment resuspension and/or gradients in settling flux. All else being equal, if the critical erosion stress is lower in a given area, then more sediment will reenter suspension there, while if the settling flux is lower, less sediment will settle back out of the water column. The area with a lower

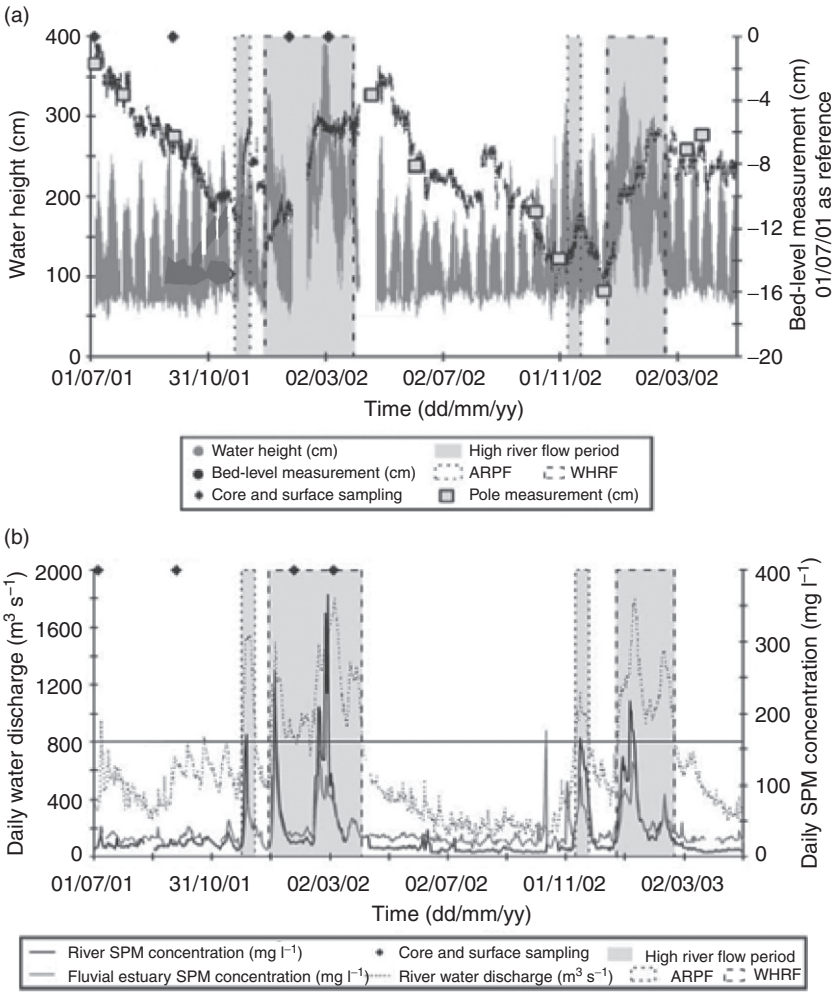

Figure 9 Time series from the upper fluvial part of the macrotidal Seine estuary, France, from 2001 to 2003. (a) Bed elevation and water levels measured on the Oissel mudflat. ARPF, autumnal rising peak flow; WHRF, winter high river flow. (b) Daily water discharge at a lock 20 km upstream of Oissel and suspended particle mass concentrations (SPM) at the lock and at an estuarine station 15 km downstream of Oissel. The horizontal line at 800 $m^3 s^{-1}$ defines WHRF. When sediment concentrations are high in the river channel, sediment flux is from the channel to the flats; when concentration is low in the river channel, flux is from the flats to the channel. Modified from Deloffre, J., Lafite, R., Lesueur, P., Lesourd, S., Verney, R., Guézennec, L., 2005. Sedimentary processes on an intertidal mudflat in the upper macrotidal Seine estuary, France. Estuarine, Coastal and Shelf Science 64, 710–720.

critical erosion stress or lower settling rate will have higher suspended sediment concentrations, and tides will tend to disperse suspended sediment away from that location. Through this mechanism, the mere presence of freshly deposited mud on the mid-to-upper flats can result in a reversal in concentration gradients, even though tidal energy may still be greater on the lower flats. Consider, for example, the transition from neap to spring tide. During neap tide, lower tidal velocity may cause mud to gradually settle without resuspension across broad swaths of the inner tidal flat. On the transition to spring tide, however, higher tidal velocity may resuspend the recently deposited mud, raising depth-averaged suspended sediment concentrations on the muddy inner flat relative to the more energetic but less turbid tidal currents flowing over the sandier lower flat.

Biological activity can locally increase or decrease bed erodibility or settling flux or both, depending on the nature of bioturbation, bioadhesion, and/or bioaggregation (e.g., Riethmüller et al., 2000; Widdows et al., 2004; Andersen et al., 2005). These biological effects can be independent of larger-scale hydrodynamics or external sediment supply and can independently affect the direction of net sediment transport (cf. **Figure 4**). **Figure 10** describes observations of greater bioaggregation and adhesion on tidal mudflats in the Kongsmark, Denmark, in summer (Andersen et al., 2005), leading to net shoreward transport from sub-tidal channels toward neighboring tidal flats and net deposition. Andersen et al. (2005) found high erosion thresholds on the mudflat at places where algal biofilms were present and low thresholds for sites dominated by small fecal pellets produced by grazing snails. Thus, algal films contributed to net deposition via a reduction in erodibility. Although fecal pellets on the flats were easier to erode than sediment on the flats covered with algal films, the pellet settling velocity

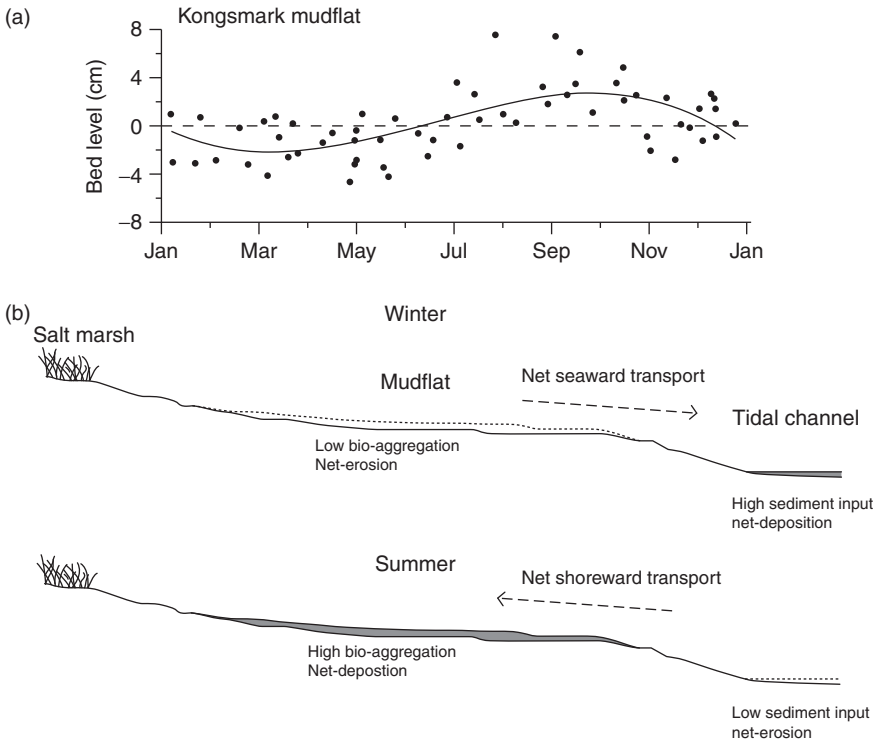

Figure 10 (a) Seasonal variation of bed level observed on the middle section for the Kongsmark tidal mudflat, Denmark. (b) Conceptual model for net transport and bed change during winter and summer at Kongsmark. Lower biological aggregation in winter results in higher erodibility on the mudflat, net erosion, and net seaward transport. During the summer, higher biological adhesion and aggregation leads to the opposite pattern. From Andersen, T.J., Lund-Hansen, L.C., Pejrup, M., Jensen, K.T., Mouritsen, K.N., 2005. Biologically induced differences in erodibility and aggregation of subtidal and intertidal sediment: a possible cause for seasonal changes in sediment deposition. Journal of Marine Systems 55, 123–138.

on the flats was much higher than the settling velocity of unpelletized mud in the neighboring subtidal channel. Thus, pellets still contributed to lowering concentration and trapping sediment on the flat via a rapid settling effect. For the York River Estuary, Virginia, USA, Friedrichs et al. (2008) found that a seasonal increase in fecal pellet concentration was associated with a decrease in erodibility as well as an increase in settling velocity.

3.06.3 Net Transport due to Eulerian Asymmetries

3.06.3.1 Definitions and Types of Eulerian Asymmetry

For cases with no spatial gradients in velocity, stress or concentration, net sediment transport can still occur over the tidal cycle in response to Eulerian (i.e., local, time-dependent) asymmetries. Examples of mechanisms which may induce tidally averaged Eulerian transport of sediment include distortion of tidal velocity away from a simple sinusoid (e.g., Friedrichs and Aubrey, 1988), a symmetric tide combined with a nonzero residual current (e.g., Nichols and Biggs, 1985), asymmetric bed stress or turbulence due to tidally varying stratification (e.g., Scully and Friedrichs, 2007), and bed slope effects (Schuttelaars and de Swart, 1999). For well-mixed tidal systems with gentle bed slopes such as tidal flats, the most important of these Eulerian asymmetry examples is usually the distortion of periodic tidal velocity (Dronkers, 1986). Coarser sediment is more sensitive to local asymmetries in maximum velocity, while fine sediment is more sensitive to local asymmetries in the duration of slack.

Because bed stress, suspension, and the resulting transport rates are all nonlinearly related to local velocity, a short but intense flood period transports more sediment landward than a long but weaker ebb period, and vice versa (Friedrichs and Aubrey, 1988), even in the presence of zero mean current (**Figure 11(a)**). Peak currents that are stronger on flood or on ebb are termed 'flood dominant' or 'ebb dominant', respectively. A simple way of conceptualizing the effect of peak velocity asymmetry is to assume that sediment suspension and transport increase with bed stress magnitude $|\tau| \sim U_T^2$ above some critical stress, τ_c. A well-mixed, flood- or ebb-dominant tidal current will tend to produce a significantly greater excess shear stress ($|\tau| - \tau_c$) during flood or ebb, respectively, favoring net sediment flux (**Figure 11(b)**). This assumption is most valid when the response of concentration to stress is instantaneous; thus, coarser sediment responds most directly to peak velocity asymmetry.

Slack duration asymmetry can also lead to Eulerian net sediment transport. Tides with a longer slack around high water than low water favor landward sediment transport because there is more time for sediment to settle out after flood (**Figure 11(c)**). Conversely, a longer slack around low tide favors seaward transport (Dronkers, 1986). Like the Lagrangian asymmetries discussed earlier, the slack duration

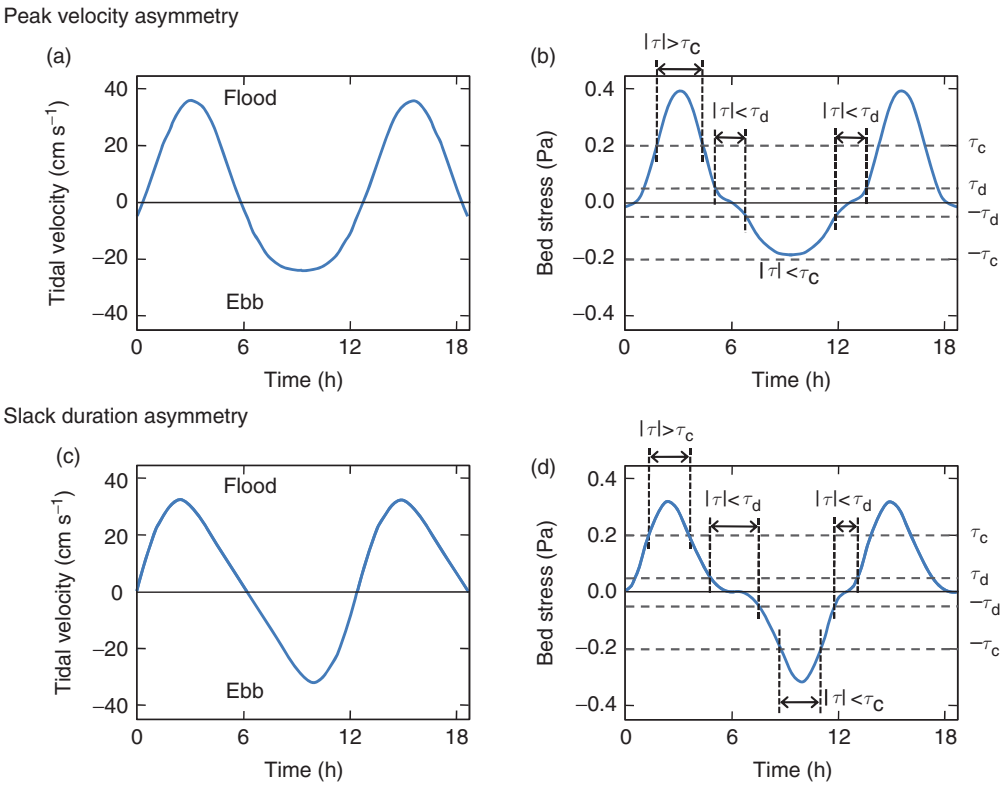

Figure 11 Idealized examples of: (a) flood-dominant current with no residual and (b) resulting asymmetry in peak stress, favoring landward sediment transport. (Ebb-dominant case would flip curves vertically.) (c) Longer duration slack after flood with no residual and (d) resulting asymmetry in periods of low stress magnitude. (Longer duration slack after ebb would flip curves horizontally.) Plots constructed with $U_T = M_2 \cos(\omega t - \theta_{M2}) + M_4 \cos(2\omega t - \theta_{M4})$, $M_2 = 30\ \mathrm{cm\ s^{-1}}$, $M_4/M_2 = 0.2$, $\omega = 1.4 \times 10^{-4}\ \mathrm{s^{-1}}$, $\tau = \rho c_d U_T |U_T|$, $c_d = 0.003$, $\rho = 1028\ \mathrm{kg\ m^{-3}}$, $\tau_d = 0.05$ Pa, $\tau_c = 0.2$ Pa, (a) and (b) $2\theta_{M2} - \theta_{M4} = 0°$, (c) and (d) $2\theta_{M2} - \theta_{M4} = 90°$.

effect relies on a time lag in the relationship between stress and concentration. As a result, finer sediment is more sensitive to duration asymmetry. A simple model for this behavior assumes that deposition is favored when $|\tau|$ is below some deposition stress, τ_d. Whichever slack has a longer period of $|\tau| < \tau_d$ will deposit more sediment (**Figure 11(d)**). By definition, tidal flats usually have a longer slack after flood because there is generally no water present during the slack after ebb. Nonetheless, sub-tidal channels that directly feed sediment to adjacent flats are likely to respond significantly to asymmetries in slack duration (Dronkers, 1986).

A temporal correlation between tidal stage and other suspension- or disturbance-inducing events can also induce net transport via local temporal asymmetries. For example, wave heights over flats tend to be highest around high water, so more sediment is suspended around slack after flood than slack after ebb, leading to seaward net transport. Conversely, rainfall disturbs tidal flat sediment more around low water (Tolhurst et al., 2006). Thus, the flood tide following a rainfall might tend to move this sediment landward – although rain-induced runoff might move it seaward. In the absence of rain, desiccation during subaerial exposure favors consolidation, conceivably reducing onshore sediment transport by the following flood. Waves, rain, and desiccation are all examples of Eulerian asymmetries that can simultaneously cause Lagrangian asymmetries – they all tend to affect the landward portion of a flat most intensely (see Section 3.06.2). The Lagrangian effect of waves reinforces the Eulerian trend; however, the Lagrangian effects of rain and desiccation may be opposite to their Eulerian tendencies.

3.06.3.2 Eulerian Velocity Asymmetries Induced by Continuity Alone

A local asymmetry in the duration of slack can be induced by the shape of a tidal flat profile, even if tidal elevation, $\eta(t)$, is perfectly sinusoidal and spatially uniform. Equation [1a] (specifically the dependence of U_T on $(x_f - x)/h$) helps explain the relationship between the shape of a tidal flat and the local duration of slack. If a flat profile is convex-up, $(x_f - x)/h$ will locally increase in magnitude as the tide rises, decreasing the duration of high-water slack and potentially reducing fine sediment deposition (**Figures 12(a)–12(c)**). Conversely, if a flat profile is concave-up, $(x_f - x)/h$ will locally decrease in magnitude approaching high water, increasing the duration of slack and increasing deposition. Similar arguments apply with regard to the convexity or concavity of a tidal embayment's overall hypsometry (the distribution of basin surface area as a function of elevation) (e.g., Pethick, 1980; Dronkers, 1986; Friedrichs, 2010). (Note that although the local duration of slack argument requires a lag between energy and

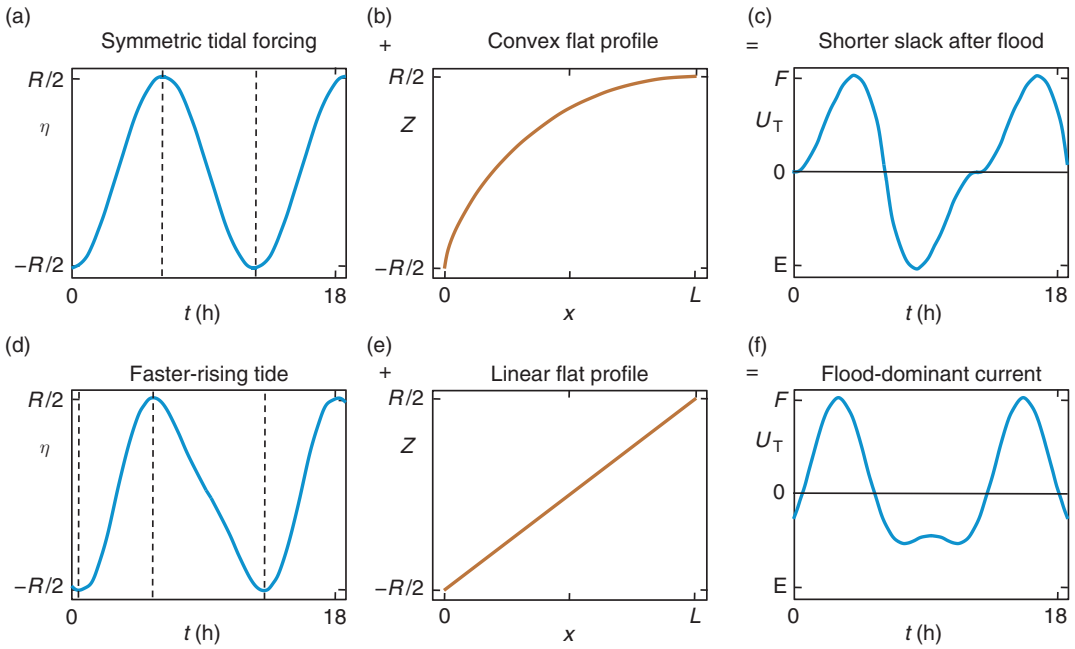

Figure 12 Tidal current based on continuity alone: if (a) tidal elevation is perfectly sinusoidal and (b) the flat profile is convex-up, then (c) the slack after flood will be shortened, potentially reducing sediment deposition. (A concave-up flat would lengthen slack after flood.) If (d) the tide rises more quickly than it falls and (e) the flat profile is linear, then (f) the tidal current will be flood dominant, increasing landward sediment transport. (If the tide falls more quickly than it rises, ebb dominance would be favored.) Plots display velocities calculated at $x = 0$.

concentration, it is defined as 'Eulerian' here because it involves a local asymmetry and does not require a spatial gradient in concentration.)

If tidal elevation at the seaward edge of a tidal flat is distorted (i.e., nonsinusoidal), Eulerian asymmetries in tidal velocity may occur over the flat itself due to the dependence of U_T on $d\eta/dt$ in eqn [1a]. In particular, if the tide rises more quickly than it falls (or vice versa), the current across the flat will tend to be flood dominant (or ebb dominant), independent of the slope of the flat (**Figures 12(d)–12(f)**). For example, the faster-rising tide found in the North Sea along the Dutch coast favors flood dominance on the neighboring intertidal Dutch Wadden Sea, contributing to the accretion of the tidal flats found there (Dronkers, 1986). If asymmetries in $d\eta(t)/dt$ and nonlinear topographic profiles or hypsometry are both present, the result can be relatively complex, stage-dependent asymmetries in Eulerian velocity (cf. Pethick, 1980).

3.06.3.3 Eulerian Asymmetries Induced by Momentum plus Continuity

For application to the tidal flats found along estuaries or embayments, the net effect of asymmetries in $\eta(t)$ generated within the estuary or embayment by the interaction of both momentum and continuity can be predicted via the tidal asymmetry parameter (Friedrichs, 2010):

$$\gamma = (1/2)(R/\langle h_c \rangle - \Delta b/\langle b \rangle) \qquad [2]$$

where R is the tidal range, h_c the channel depth, b the embayment width including intertidal areas, Δb the amplitude of tidal variation in width, and $\langle\,\rangle$ indicates a tidal average. $R/\langle h_c \rangle$ and $\Delta b/\langle b \rangle$ scale the importance of nonlinearities induced by tidally varying channel depth and tidally varying embayment width, respectively. If an embayment is characterized by a negative asymmetry parameter ($\gamma < 0$) such that $\Delta b/\langle b \rangle$ is greater than $R/\langle h_c \rangle$, then the filling and draining of intertidal areas will slow the landward propagation of high tide relative to low tide (Friedrichs, 2010). Low tide will partially catch up with high tide, and the temporal transition from high to low water will be shortened. The result will be a quicker falling tide and a tendency toward ebb dominance over the flats. Conversely, if the embayment is characterized by a positive asymmetry parameter ($\gamma > 0$) such that $R/\langle h_c \rangle$ is greater than $\Delta b/\langle b \rangle$, tidal propagation along shallow channels will delay low tide, and high tide will move faster. The tide will become quicker rising, and flood dominance will be favored across the flats.

If tidal flats are sufficiently wide, spatial gradients in $\eta(x,t)$ across the flats themselves can significantly affect Eulerian asymmetries. Dynamically, a tidal flat has much in common with a wide and shallow tidal channel, in that high tide propagates landward more quickly than low tide, favoring flood dominance. Thus, if a tidal flat is forced at its seaward edge by a symmetric tide, the tide eventually becomes faster rising and increasingly flood dominant with landward distance, forming a tidal bore in the extreme of a very wide macrotidal flat (Dronkers, 1986; **Figure 13(a)**). Even if a tidal flat is forced by a faster-falling tide such that it is ebb dominant at its seaward edge, a sufficiently wide flat will cause the landward tide to eventually become faster rising and flood dominant (Friedrichs et al., 1992). Conversely, the likelihood of ebb dominance at the seaward edge of tidal flats is enhanced by the locally large pressure gradients that develop there near low water (Dronkers, 1986; **Figure 13(b)**).

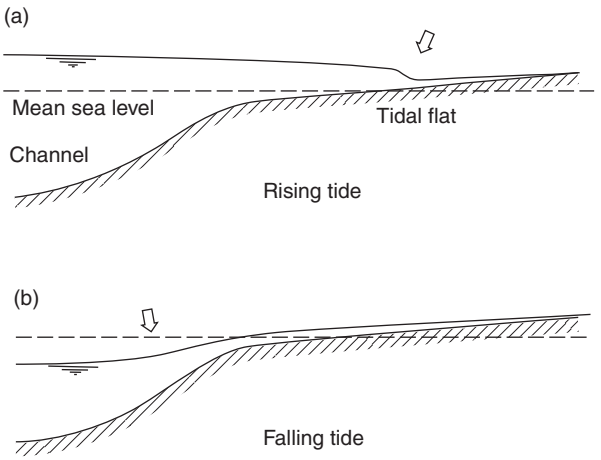

Figure 13 Spatial gradients in $\eta(x,t)$ can affect Eulian asymmetry across wide flats. (a) Flood dominance is favored by the development of tidal bores (arrow) over inner flats during the rising tide. (b) Ebb dominance is favored by locally large pressure gradients (arrow) over outer flats during the falling tide. Modified from Dronkers, J., 1986. Tidal asymmetry and estuarine morphology. Netherlands Journal of Sea Research 20, 117–131.

3.06.3.4 Observations of Eulerian Asymmetries and Resulting Sediment Transport

Locally, velocity (and, therefore, bed stress) across tidal flats is constrained by continuity to respond to the rate at which the water surface rises or falls (see eqns [1a]–[1c]). On the upper flat, this favors a tendency for Eulerian velocities and stresses due to tides to be greatest near the tidal front, that is, soon after the tidal flat is first submerged during flood and just before the tidal flat is finally exposed on ebb. **Figure 14** provides observed examples of this characteristic velocity distortion pattern from the macrotidal mudflats of the Wash, UK (Collins et al., 1998) and Marennes-Oléron Bay, France (Le Hir et al., 2000) (for a numerical example, see hours 4.5–7.5 in **Figures 15(b)** and **15(d)**.) On upper flats, the continuity constraint favoring this characteristic velocity spike near the tidal front on both flood and ebb results from the fact that the sinusoidal rate of sea-level change around high tide is inversely proportional to water depth. On flood, this velocity spike may be reinforced by momentum-induced bores associated with strong frictional nonlinearities in the immediate vicinity of the tidal front where water depths are small. Such bore-like behavior causes the water surface to rise faster on flood and fall slower on ebb. From local observations of flood dominance, such as those seen in **Figure 14**, it is difficult to determine if the associated quicker-rising Eulerian distortion in the surface elevation (also apparent in **Figure 14**) is primarily the result of local bore-like behavior, or if the quicker-rising surface elevation is mainly forced by distortions in the neighboring estuarine or coastal ocean tide. In either case, the flood velocity spike on the flat will still be accentuated relative to the ebb in response to local continuity constraints.

Observations from the Hythe flats, Southampton Water, UK (**Figure 16**; Quaresma et al., 2007), illustrate several key features common to tidally dominated sediment transport

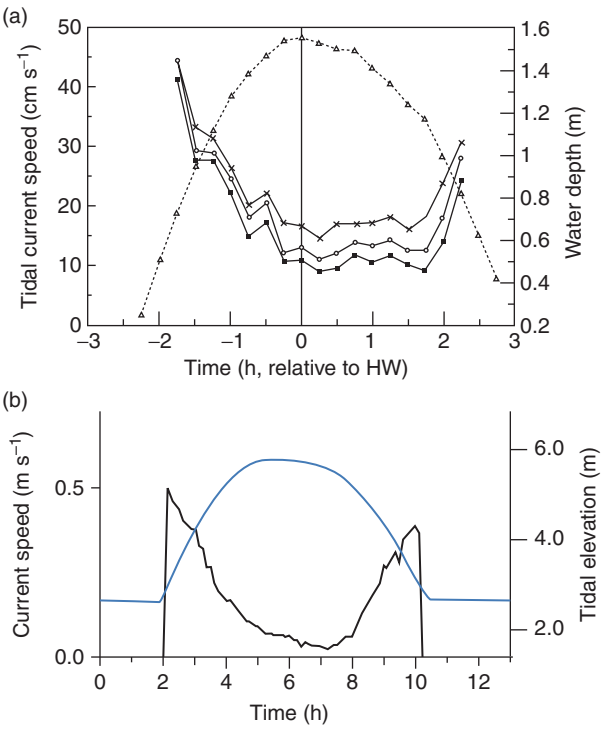

Figure 14 Time series of tidal elevation and current speed over macrotidal mudflats at (a) the Wash, UK, in September 1980 (at 10, 25, and 63 cm above the bed); and (b) the Brouage flat, Marennes-Oléron Bay, France, in November 1994 (at 32 cm above the bed). Maxima in tidal velocity occur soon after the flat is first submerged on flood and just before it is exposed on ebb. Also, a quicker-rising flood is associated with a stronger velocity spike at the beginning of flood. (a) Modified from Collins, M.B., Ke, X., Gao, S., 1998. Tidally-induced flow structure over intertidal flats. Estuarine Coastal and Shelf Science 46, 233–250. (b) Modified from Le Hir, P., Roberts, W., Cazaillet, O., Christie, M., Bassoullet, P., Bacher, C., 2000. Characterization of intertidal flat hydrodynamics. Continental Shelf Research 20, 1433–1459.

across tidal flats. In response to the Eulerian velocity and bed stress spikes characteristic of the tidal front on both flood and ebb (**Figures 14** and **16(b)**), a corresponding double peak in suspended sediment concentration is typically observed (**Figure 16(c)**). Because sediment transport is the product of velocity and concentration, the spikes in sediment transport at the tidal front tend to be even more extreme that those in velocity or stress **Figure 16(d)**). The observations in **Figure 16** confirm the tendency that, on most tidal flats and in the absence of significant waves, tidal processes alone usually lead to net landward sediment transport (landward is negative in **Figure 16(d)**). However, these observations also illustrate how difficult it is to conclusively separate the effects of Eulerian and Lagrangian asymmetries in observations. The dominance of landward transport in **Figure 16(d)** is probably also due at least in part to the fact that tidal velocities and stresses are stronger in the neighboring sub-tidal Southampton Water than on the Hythe flats themselves. Another key point highlighted by the Hythe flat observations is that on natural tidal flats, particularly those along the edges of tidal estuaries and tidal rivers, the along-shore component of current speed

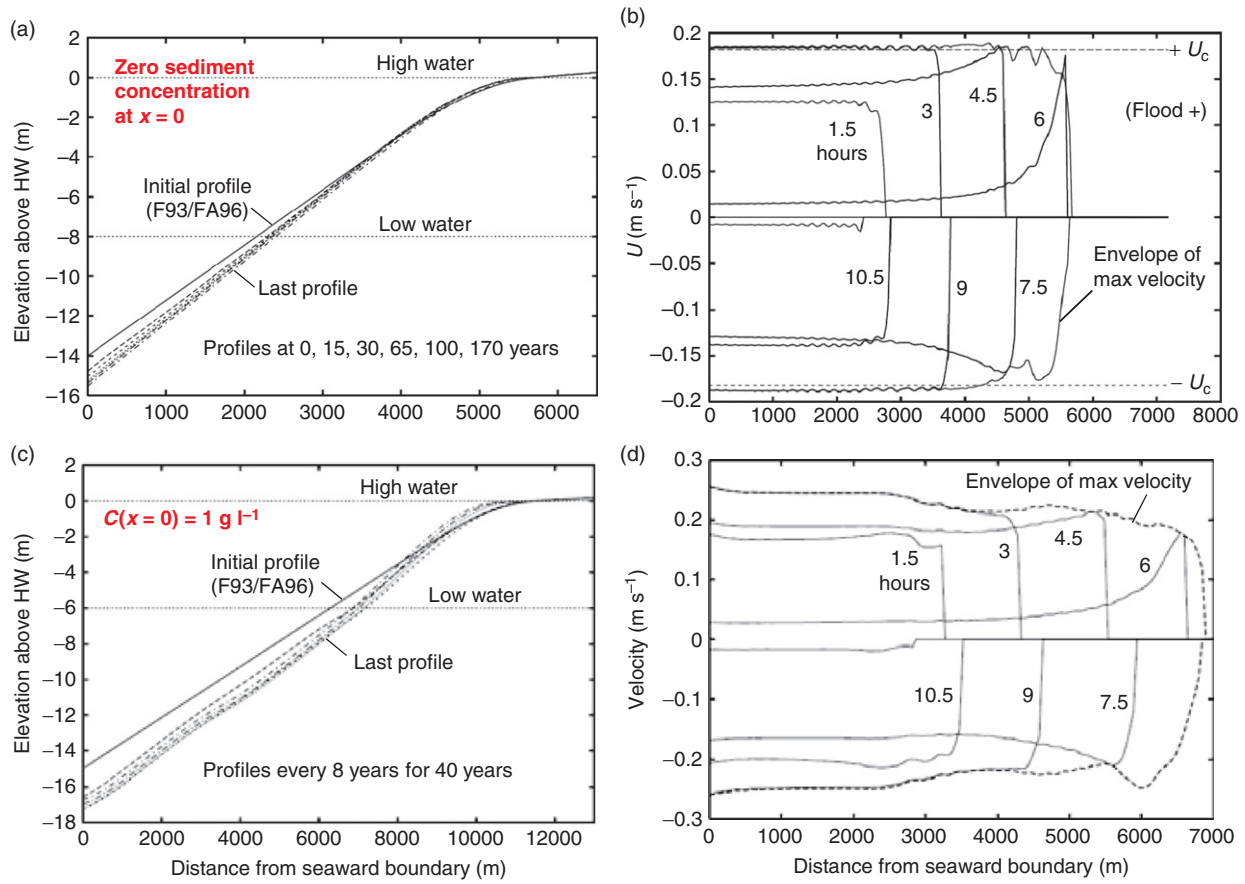

Figure 15 Results from a 1-D sediment transport model forced by a sinusoidal semi-diurnal tide with (a) and (b) $C(x=0)=0$, $R=8$ m, and (c) and (d) $C(x=0)=1$ g l^{-1}, $R=6$ m. (a, c) Profile evolution with initial profile (solid line) set to F93/FA96 solution. (b, d) Velocity snapshots at 1/8 tidal period intervals and envelope of maximum flood and ebb velocity for last profile. Also shown in (b) is $+/-U_c$, their choice for the critical velocity for sediment erosion. Numerical sediment transport experiments with sinusoidal tidal forcing alone produce final equilibrium profiles relatively similar to the initial form set to the F93/FA96 analytical result and tend to exhibit maximum tidal velocities and bed stresses that are nearly uniform in space. With $C(x=0)$ the equilibrium profile is eventually fixed in space, while for $C(x=0)>0$, the equilibrium profile shape continually progrades seaward. Modified from Pritchard, D., Hogg, A.J., Roberts, W., 2002. Morphological modeling of intertidal mudflats: the role of cross-shore tidal currents. Continental Shelf Research 20, 1887–1895.

and sediment transport (**Figures 16(b)** and **16(d)**) tend to be just as strong, if not stronger, than the across-shore components. Along-shore currents are also present to some degree in the velocity observations from the Wash ((**Figure 14(a)**) because the current speed never drops below ~10 cm s^{-1} at high tide.

3.06.4 Theoretical Equilibria in Response to Tides, Waves, and Sediment Supply

3.06.4.1 Convex-Up Profile in Response to Uniform Maximum Tidal Velocity

As net sediment transport by lag effects are reduced if there are no spatial variations in bed stress, a logical candidate for an equilibrium tidal flat profile subject to symmetric Eulerian forcing of tidal elevation and velocity is where the bathymetry minimizes the spatial variations in velocity. Friedrichs (1993) and Friedrichs and Aubrey (1996) (hereafter F93/FA96) presented analytical solutions for this type of profile for cases subject to either tides alone or waves alone. For the tides alone case, F93/FA96 inverted eqns [1a]–[1c] to solve for $Z(x)$ such that the maximum value for U_T over the tidal cycle was constant in space. For the case of a straight shoreline, the equilibrium solution of F93/FA96 resulted in a profile which is linear between low water and mean tide level, and above mean tide is convex-up as predicted by

$$Z(x) = (R/2)\sin\ (x/L^{*}-1)\ \text{for}\ x > L^{*} \qquad [3a]$$

where Z, x, and R are defined as in **Figure 5**. The horizontal distance between the low water and mean tide levels, L^{*}, is given by

$$L^{*}=L/(\pi/2+1) \qquad [3b]$$

where L is the total width of the intertidal flat. The maximum across-shore component of tidal velocity everywhere over the profile is then

$$U_{\mathrm{TMAX}} = L^{*}\omega = L\omega/(\pi/2+1) \qquad [3c]$$

Besides neglecting Eulerian asymmetries, this approach assumes that maximum velocity is more important than the duration of slack or depth-dependent settling in determining

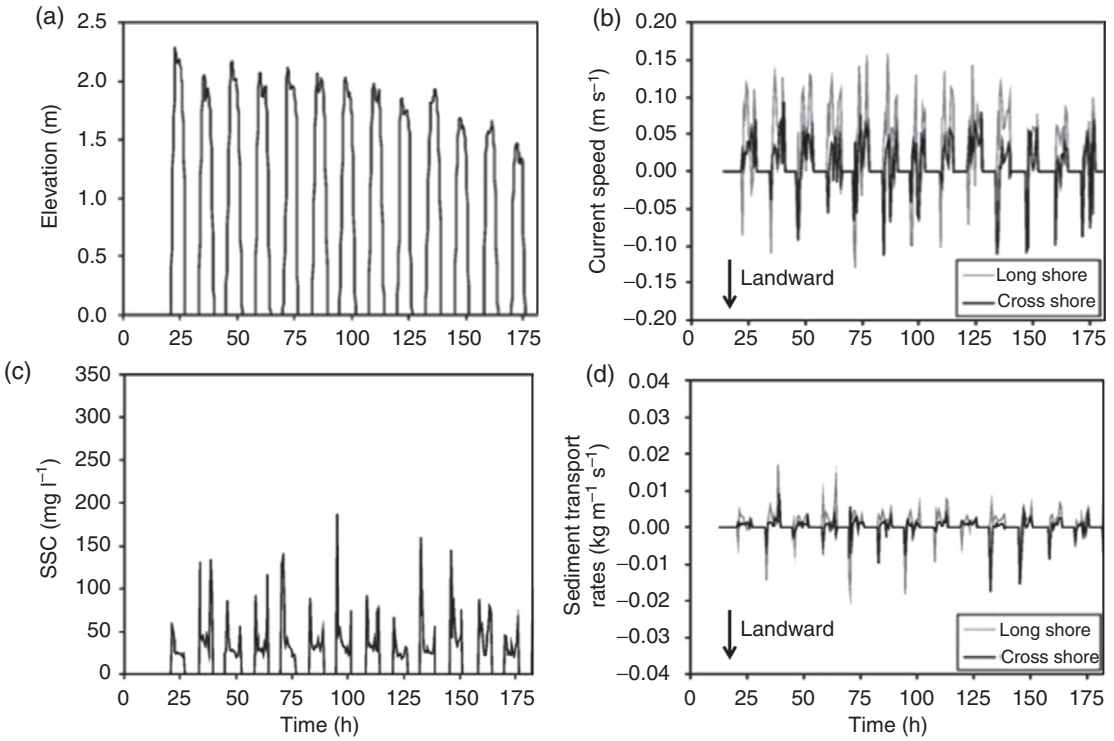

Figure 16 Time series from the Hythe mudflat adjacent to the Southampton Water estuary, UK, in June 2000 of (a) tidal elevation, (b) tidal velocity (along-shore is gray and positive toward the estuary mouth; across-shore is black and negative landward), (c) suspended sediment concentration, and (d) sediment transport (definitions as in (b)). Characteristic double spikes occur near the tidal front in suspended sediment concentration and transport. Modified from Quaresma, V.S., Bastos, A.C., Amos, C.L., 2007. Sedimentary processes over an intertidal flat: a field investigation at Hythe flats, Southampton Water (UK). Marine Geology 241, 117–136.

equilibrium morphology. F93/FA96 also considered the effect of flow convergence or divergence due to an embayed or a lobate coastline. They further noted that the trends predicted by their solutions still held in the presence of an along-shore current as long as the strength of this current was proportional to the strength of the across-shore current. If along-shore currents are proportional to across-shore currents, then L in eqns [3a]–[3c] becomes the dimension of the flat in the direction of maximum velocity, and the across-shore width of the flat reduces to $L_x = L\cos\theta$, where θ is the angle between the maximum tidal velocity and the shoreline.

The equilibrium profiles derived by F93/FA96 under sinusoidal tidal forcing are convex-up and become more convex as the coastline becomes more embayed (**Figure 17**). Assuming uniform maximum tidal velocity (i.e., maximum bed stress) to be key, the profile convexity at equilibrium is due to the proportionality between tidal velocity and the rate at which tidal elevation is changing (i.e., $U_T \sim [(x_f - x)/h]\, dh/dt$ in eqn [1a]). Since $d\eta/dt$ becomes smaller approaching high water, the bed slope near the tidal front, $|dh/dx_f|$, must simultaneously decrease in order to increase the magnitude of $(x_f - x)/h$. If the shoreline is embayed, still more profile convexity is needed to compensate for the tendency of tidal velocity to further slow down as the flow laterally diverges.

Numerical sediment-transport experiments with sinusoidal tidal forcing alone produce convex-up equilibrium profiles relatively similar to the F93/FA96 analytical result (**Figures 15(a)** and **15(c)**; Roberts et al., 2000; Roberts and Whitehouse, 2001; Pritchard et al., 2002; Pritchard and Hogg, 2003; Waeles et al., 2004). All of these authors employed one-dimensional (1-D) hydrodynamic and advective transport equations with erosion $\sim(\tau - \tau_c)$ and deposition $\sim(\tau_d - \tau)$, where $\tau = \rho c_d U_T^2$ is the bed stress, ρ the water density, and c_d a drag coefficient – although Pritchard and Hogg (2003) also showed that the resulting equilibrium shape was insensitive to the specific formulations for erosion and deposition. For a case with a seaward boundary condition of zero suspended sediment concentration (C), Pritchard et al. (2002) found that the tidal flat evolved to an equilibrium condition such that maximum tidal velocity was everywhere nearly uniform and equal to the critical velocity (U_c) which produced $\tau = \tau_c$ (**Figure 15(b)**). Once this condition was reached, the shape of the tidal flat profile became constant in time, and its position remained stationary in space.

3.06.4.2 Equilibrium Shape in Response to Tidal Range and Sediment Supply

The numerical models described in Section 3.06.4.1 all predict that if offshore concentration is held fixed but tidal range is varied, the width of tidally dominated flats at morphological equilibrium will remain more or less constant and be nearly independent of tidal range. The convex profile shape remains similar to the F93/FA96 solution, and the width remains nearly fixed, but the slope of the idealized flats increases linearly with tidal range (**Figure 18(a)**). This theoretical result can be easily

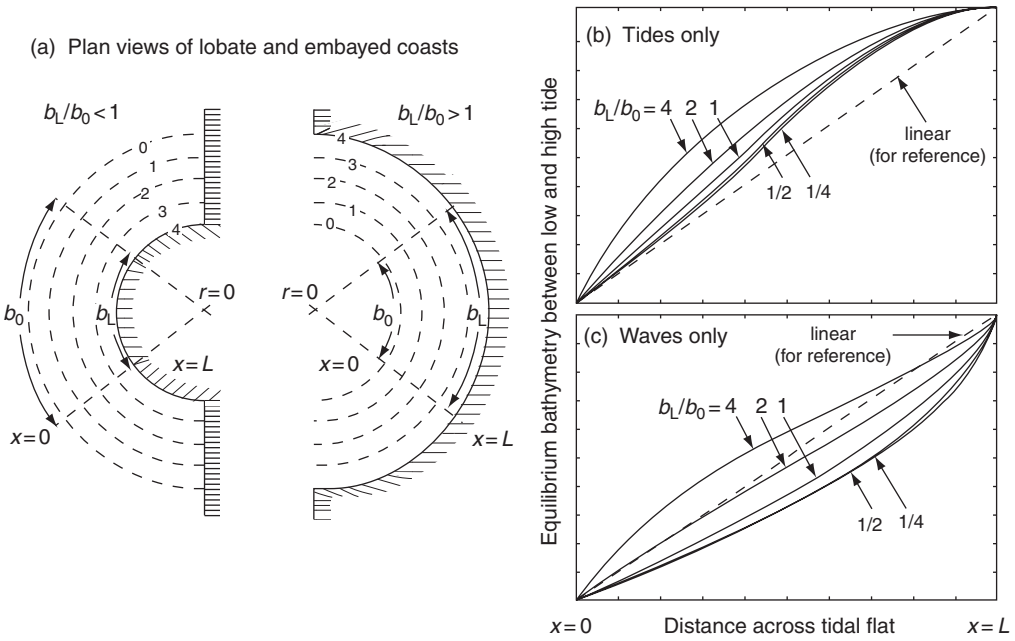

Figure 17 (a) Schematic plan view of a lobate and an embayed tidal flat coastline. The contours 0–4 are arbitrary elevations between low and high water. Analytical solutions for equilibrium bathymetric profiles between low and high water which result in spatially uniform maximum velocities for (a) tides only and (b) waves only. Tides and embayed coastlines favor convex-up flats, whereas waves and lobate coastlines favor concave-up flats. Modified from Friedrichs, C.T., Aubrey, D.G., 1996. Uniform bottom shear stress and equilibrium hypsometry of intertidal flats. In: Pattiaratchi, C. (Ed.), Mixing Processes in Estuaries and Coastal Seas. American Geophysical Union, Washington, DC, pp. 405–429.

understood by further examining eqns [3b] and [3c], the F93/FA96 analytical solutions for equilibrium flat width and the maximum across-shore component of tidal velocity. Assuming a constant tidal period and that stability is set by some externally fixed critical value of $U_{TMAX} = U_c$, with $U_{TMAX} = L\omega/(\pi/2+1)$, then the equilibrium width of a tidal flat subject only to across-shore tidal currents will not vary with tidal range. The slope of the flat, however, is given approximately by

$$\text{Slope} \approx R/L = R\omega/((\pi/2+1)U_c) \qquad [4a]$$

Therefore, if U_c is externally fixed, idealized tidal flats become steeper as tidal range increases (because L must remain constant to keep U_c constant).

By contrast, changing sediment supply, as parametrized by various suspended sediment concentrations, C, imposed at the seaward boundary, leads to distinctly different equilibrium widths, L, for tidally dominated flats (Roberts et al., 2000; **Figure 18(b)**). (Nonetheless, a convex-up shape similar to that predicted by the F93/FA96 solution is still retained – see **Figure 15(c)**.) This trend of increasing width with increasing concentration can be understood via further examination of eqn [3c], that is, that at equilibrium

$$L = (\pi/2+1)U_c/\omega \qquad [4b]$$

and the critical stability velocity, U_c, increases with externally imposed sediment concentration. According to the conceptual argument presented in **Figures 3** and **4**, morphological equilibrium is likely to be prevented in dispersive systems if strong spatial gradients in suspended sediment concentration persist. Therefore, if the magnitude of C imposed at the seaward boundary of a tidal flat is increased, it follows that morphological equilibrium should favor a form that generates similarly high concentrations across the entire profile (Pritchard et al., 2002). For tides alone, a larger, nearly uniform C across the entire flat requires a larger, nearly uniform U_c. Equation [4b] indicates that tidal flat width, L, at equilibrium is proportional to U_c, such that if C imposed at the mouth increases, equilibrium flat width must also increase.

3.06.4.3 Equilibrium in Response to Persistent Tidal Asymmetries

Pritchard et al. (2002) and Waeles et al. (2004) both found that for sinusoidal forcing and a nonzero sediment concentration imposed at the seaward boundary ($C(x=0)>0$), the equilibrium profile shape prograded slowly seaward with time (see **Figure 15(c)**), a pattern Pritchard et al. (2002) attributed to weak but persistent asymmetries within the system. They argued that the noninstantaneous response between sediment concentration and bed stress meant that tidally averaged settling lag was not quite zero, and the result was a small net import of sediment, even after the shape of the translating profile stopped evolving. An additional explanation for net equilibrium import of sediment under sinusoidal forcing, however, is the internal generation of flood-dominant asymmetry due to bore-like tidal wave distortion (Friedrichs et al., 1992) as discussed in Section 3.06.3.3 and as illustrated in **Figure 13(a)**. It is worth noting that both Pritchard et al. (2002) and Waeles et al. (2004), who found net sediment import at equilibrium, included momentum in their hydrodynamic component (needed for bore-like distortion), whereas Roberts et al. (2000), who found no net

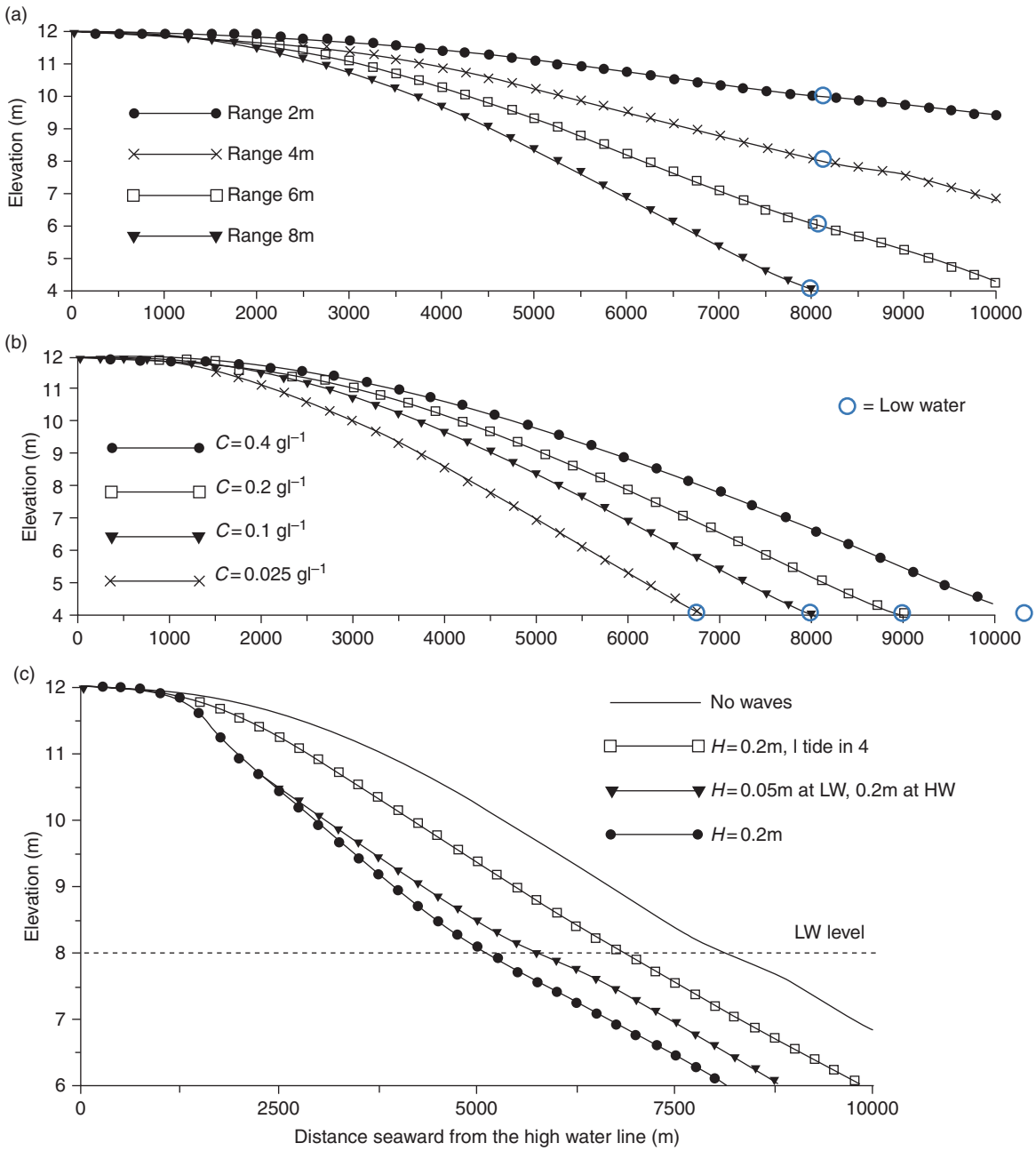

Figure 18 Equilibrium profiles predicted by a 1-D sediment transport model forced by a sinusoidal semi-diurnal tide with $\tau_c = 0.2$ Pa, $\tau_d = 0.1$ Pa. (a) Tide only, $C(x=0) = 0.1$ g, $R = 2, 4, 6, 8$ m; (b) tide only, $R = 8$ m, $C = 0.025, 0.1, 0.2, 0.4$ g; (c) tide plus waves, $R = 4$ m, $C(x=0) = 0.1$ g, and various shallow-water wave forcings as indicated in the figure's legend with H limited to 50% of water depth. Steepness increases with tidal range (R), width increases with sediment concentration (C), and concavity increases with the influence of wave height (H). See text for further discussion. Modified from Roberts, W., Le Hir, P., Whitehouse, R.J.S., 2000. Investigation using simple mathematical models of the effect of tidal currents and waves on the profile shape of intertidal flats. Continental Shelf Research 20, 1079–1097.

sediment import at equilibrium, based their hydrodynamics on continuity alone.

Pritchard et al. (2002) also used their 1-D sediment-transport model to examine the effect on tidal flat profiles of flood- and ebb-dominant currents arising from seaward forcing by quicker-rising or quicker-falling tides (cf. **Figure 12(d)**). The first morphological effect they associated with this type of Eulerian forcing asymmetry was increased profile steepness. As indicated by eqn [2], continuity causes tidal velocity to be proportional to the rate of change in tidal elevation, that is, $U_T \sim d\eta/dt$. Thus, a tide that is quicker rising or quicker falling will have a greater maximum $|d\eta/dt|$ and, therefore, a greater U_{TMAX} than a sinusoidal tide of the same tidal range acting on a flat of the same width and shape. To reduce U_{TMAX} to a value consistent with an externally set U_c or $C(x=0)$, L at equilibrium must be reduced relative to its sinusoidally forced equivalent.

Both ebb- and flood-dominant flats at equilibrium are therefore narrower and steeper than the symmetrically forced case. For cases with $C(x=0)>0$, the second morphological effect Pritchard et al. (2002) associated with asymmetric seaward forcing is enhanced net migration of the equilibrium profile. Quicker-rising tides/flood dominance leads to faster progradation, and quicker-falling tides/ebb dominance can lead to recession.

Eulerian tidal asymmetries produced by finite channel depth and intertidal storage in tidal embayments (scaled by as $\gamma = (R/\langle h_c\rangle - \Delta b/\langle b\rangle)/2$, as described in Section 3.06.3.3) can lead to morphodynamic feedbacks which control further evolution of both sub-tidal and intertidal areas (Boon and Byrne, 1981; Dronkers, 1986; Friedrichs and Aubrey, 1988; Friedrichs et al., 1992; Pethick, 1996). For example, a small tidal flat (i.e., $\gamma>0$) lying at a relatively low elevation relative to mean water tends to favor both system-wide flood dominance and a longer period of slack after flood (Friedrichs, 2010). Flood dominance and an extended slack after flood then favor sediment import and settlement, and tidal flats are more likely to accrete. However, as tidal flats expand and rise higher above mean tide level (with $\Delta b/\langle b\rangle$ becoming greater than $R/\langle h_c\rangle$ and γ becoming negative), ebb dominance as well as a shorter slack after flood are eventually favored (Friedrichs, 2010). Sediment is then less likely to settle and more likely to be exported, and tidal flats may erode. This negative feedback mechanism suggests that an extent of tidal flats which produce $\Delta b/\langle b\rangle \approx R/\langle h_c\rangle$ (i.e., $\gamma\approx 0$) are likely to favor stability. Long-term simulations of tidal embayment evolution in the absence of waves favor this pattern such that a stable combination of tidal flats and sub-tidal channels are found to be marked by relatively small asymmetries in both (1) flood versus ebb duration and (ii) flood versus ebb peak velocity (van der Wegen et al., 2008).

3.06.4.4 Concave-Up Equilibrium in Response to Waves

Although tidal processes alone can theoretically account for the morphology of tidal flats following deposition, tidal flat profiles during times of erosion are more often dominated by waves (Pethick, 1996). For the case of bottom stress induced by waves alone, F93/FA96 incorporated conservation of energy with dissipation by bottom friction such that wave shoaling could increase or decrease the wave height used in eqn [1b]. They then inverted the equation to solve for $h(x)$ at high tide while keeping U_W constant in space. For waves alone, a straight coastline then produces a concave-up equilibrium profile (see **Figure 17(c)**) given by

$$h(x)/h_0 = (1-x/L_w)^{2/3} \qquad [5a]$$

A concave profile results in the F93/FA96 wave-dominated case because under their highly frictional shoaling, orbital velocity is proportional to $h^{1/2}$ dh/dx (for additional details see the derivation within F93/FA96). It then follows that since h decreases toward shore, $|dh/dx|$ must increase toward the shore to keep U_W constant (from eqn [1b], we see that constant U_W means wave height, H, decreases continually toward shore, further highlighting the assumption of strongly dissipative conditions). If the shoreline is embayed as in the right-hand side of **Figure 17(a)**, the profile shape must initially be steeper offshore to compensate for refraction because stronger refraction there (where the bathymetry is most tightly curved) leads to more wave energy divergence.

In eqn [5a], the depth and width scales, h_0 and L_w, are tied to the spatially uniform critical wave orbital velocity amplitude, $U_W = U_c$, and to the offshore wave height at $x=0$, H_0, via

$$L_w = (3\pi {H_0}^3 g^2)/(32 f_w {U_c}^4) \qquad [5b]$$

$$h_0 = ({H_0}^2 g)/(4{U_c}^2) \qquad [5c]$$

where f_w is the wave friction factor, and g the acceleration due to gravity. Landward of h_0, the local depth and slope of the flat will be independent of H_0 and can be re-expressed via rearranging eqns [5a]–[5c] to be a function of U_c, the remaining distance from the shoreline (x'), and the wave friction factor (f_w):

$$h(x') = \left[(4 f_w U_c)/(3\pi g^{1/2})\right]^{2/3} (x')^{2/3} \qquad [6]$$

The offshore extent (L_w) of the equilibrium dissipative profile in eqns [5a]–[6] is set by the depth, h_0, at which the offshore wave height is first capable of creating bottom orbital velocities U_W equal to the critical value of U_c.

3.06.4.5 A Solution to Predict Tidal Flat Width in Response to Waves

F93/FA96 equated h_0 with the tidal range, R, such that L_w gave the equilibrium width of the tidal flat. However, here it is suggested that h_0 is more properly set by U_c and H_0, not by R. Rather than $h_0 = R$, as assumed by F93/FA96, it may be more generally applicable to separately consider two cases, a small tidal range case with $R \le h_0$, and a large tidal range case with $R > h_0$. Using eqn [5c] to eliminate h_0, this distinction can be equivalently re-expressed as $R \le ({H_0}^2 g)/(4{U_c}^2)$ versus $R > ({H_0}^2 g)/(4{U_c}^2)$. For a small tidal range, R, the width of the intertidal portion of the flat, L, is then controlled directly by the externally imposed tidal range via its role in determining the point where $h = R$ as predicted by eqn [6]:

$$L \approx (3\pi g^{1/2} R^{3/2})/(4 f_w U_c) \text{ for } R \le ({H_0}^2 g)/(4{U_c}^2) \qquad [7a]$$

Equation [7a] predicts that the width of a high-energy, wave-dominated tidal flat will increase (and the average slope of the flat will decrease) with increased tidal range (R), decreased friction factor (f_w), and decreased critical orbital velocity (U_c). The result that L decreases as f_w or U_c increases suggests that more dissipation by bedforms or fluid mud, lower local sediment mobility, and/or higher offshore sediment concentration are likely to decrease the equilibrium width.

It may seem counterintuitive that the equilibrium tidal flat width derived above for the small R case does not increase with offshore wave height, H_0. However, for the large R case, a strong dependence on H_0 is seen. For an erosional, wave-dominated flat with $R > h_0$, the width of the erosional platform cutting into the shoreline at high water will be limited to a width of order $L \approx L_w$ (i.e., erosion will be limited to the region where U_W has grown to reach U_c):

$$L \approx (3\pi {H_0}^3 g^2)/(32 f_w {U_c}^4) \text{ for } R > ({H_0}^2 g)/(4{U_c}^2) \qquad [7b]$$

From eqn [7b] we see that in this case $L \sim {H_0}^3$, and thus with wave-dominated conditions combined with larger tidal ranges, the width of the wave-dominated tidal flat will indeed increase

strongly with offshore wave height H_0. Note that the trend in the dependence of equilibrium tidal flat width on f_w and U_c is similar for the low- and high-tidal-range cases, but the sensitivity to the critical velocity for stability is much stronger for the large tidal range case ($L \sim {U_c}^{-4}$). This suggests that the equilibrium width of wave-dominated macrotidal flats may be quite sensitive to sediment mobility, with the width of easily eroded flats being significantly greater than that for well-consolidated flats.

3.06.4.6 Theoretical Predictions of Equilibrium Slope under Wave Dominance

The equilibrium profile described by eqn [6], which assumes wave energy at high water is strongly dissipated by bottom friction, may apply most directly to open coasts bordered by shallow sub-tidal flats containing fluid mud, similar to conditions documented at times on the Surinam coast north of the Amazon (Wells and Kemp, 1986) and on the Gulf of Mexico coast west of the Mississippi (Lee and Mehta, 1997; Kineke et al., 2006). In the latter case, the resulting profile is arguably a mudshore rather than a tidal flat (cf. Mehta, 2002). Nonetheless, such a well-documented environment provides a convenient prototype against which to test the possible validity of this asymptotic theory. Based on observations of wave damping over thin layers of fluid mud off Louisiana and Texas, Kineke et al. (2006) found the wave friction factor f_w to be on the order of ~0.1. A reasonable U_c for erosion by waves of mud recently consolidated from fluid mud is $U_c \approx 35\ \mathrm{cm\ s^{-1}}$ (e.g., Friedrichs and Scully, 2007; Ma et al., 2010). **Figure 19** displays the bathymetric profile predicted by substitution of these literature-based values for f_w and U_c into eqn [6]. Thus for soft mud the slope of wave-dominated tidal flats is expected to be on the order of $0.001 < \mathrm{d}h/\mathrm{d}x < 0.01$.

Le Hir et al. (2000), like F93/FA96, applied the 1-D wave energy conservation equation with bottom friction to shallow-water waves propagating across tidal flats. They noted that if one assumes that an asymptotic limit exists for the ratio of local wave height to water depth (H/h) for highly dissipative waves, the result is a proportionality between H/h and bed slope ($\mathrm{d}h/\mathrm{d}x$) divided by the wave friction factor (f_w). With the assumption of a profile with nearly uniform U_c as described by eqn (6), solving for H/h as a function of $\mathrm{d}h/\mathrm{d}x$ and f_w becomes particularly straightforward and yields

$$H/h = (\mathrm{d}h/\mathrm{d}x)(9\pi)/(4f_w) \quad [8]$$

Observations of the relationship between observed H/h and $\mathrm{d}h/\mathrm{d}x$ can then be used as another test of the potential validity of the F93/FA96 approach (see Section 3.06.5.2).

For sand, f_w is typically smaller than for the fluid mud case discussed above – on the order of ~0.01 (e.g., Nielsen, 1992). The slope of wave-dominated sandy tidal flats dominated by dissipation via bed friction would therefore be expected to be gentler – on the order of $\sim 10^{-4}$–10^{-3}. However, sandier shores are also arguably more prone to depth-limited wave breaking, which might tend to produce steeper beach-like features. In terms of overall trends, it is reassuring to note that when applied to depth-limited breaking on sandy beaches, equilibrium profiles based on uniform energy dissipation arguments also consistently produce concave-up profiles (Larson et al., 1999). Other assumptions behind the F93/FA96 solution are also somewhat restrictive, including consideration only of shallow-water waves present at high water. Wave asymmetry during shoaling and breaking, which was entirely neglected by F93/FA96, may also play a role in the development of characteristic profiles for both muddy and sandy shores (Allison et al., 1995; Larson et al., 1999).

3.06.4.7 Predictions of Equilibria in the Presence of Waves, Tides, and Sediment Supply

1-D combined hydrodynamic and sediment-transport models have been used to model equilibrium tidal flat profiles in the presence of both waves and tidal currents without limiting solutions to times around high tide (Roberts et al., 2000;

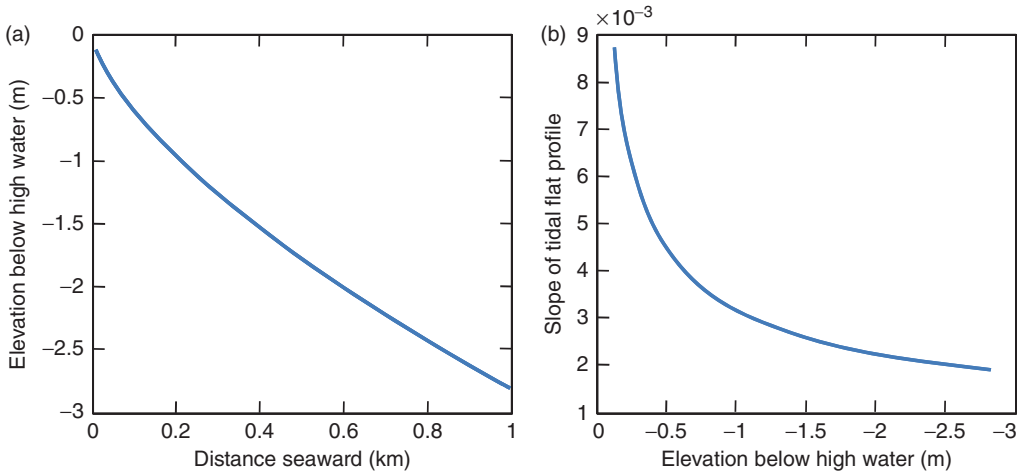

Figure 19 Equilibrium (a) profile elevation (b) profile slope predicted by eqn [6] for a highly dissipative mudflat with a wave friction factor of $f_w = 0.1$ and critical sediment mobilization velocity of $U_c = 35\ \mathrm{cm\ s^{-1}}$. The resulting equilibrium slopes between 0.01 and 0.001 are the same order of magnitude as those seen in the observed concave-up tidal flat profiles in **Figures 22** and **23**.

Waeles et al., 2004). Roberts et al. (2000) assumed shallow-water waves, whereas Waeles et al. (2004) accounted for orbital decay with depth. In both their models, maximum wave height was controlled via depth-limited breaking, whereas in the Waeles et al. (2004) case, wave height also shoaled and frictionally decayed following conservation of wave energy. Both authors then calculated total bottom stress as the sum of the contribution from tidal currents and waves. The simulations of both authors predict that the convex-up equilibrium profile for tidal flats becomes progressively more concave as wave energy increases (see **Figure 18(c)**), especially near the high-water line. A key result of Waeles et al. (2004) is that the addition of waves favors offshore sediment transport that can counteract the net import associated with symmetric tides alone. The 1-D modeling of Waeles et al. (2004) suggests that reasonable combinations of large tides and small waves lead to a stable equilibrium form that no longer progrades or recedes, but rather remains stationary in space.

Building on the results of Mehta et al. (1996), Kirby (2000, 2002) used the asymptotic tidally dominated and wave-dominated profiles of F93/FA96 as end members within a provisional conceptual model for characteristic shapes of mudflat and mudbank profiles under varying degrees of forcing by waves, tides, and sediment supply. They characterized intermediate profiles as having a stability number

$$S = 1 - F_S/F_D \quad [9]$$

where F_S and F_D are the sum of the stabilizing and destabilizing forces involved. They proposed that low hydrodynamic energy and high sediment supply contribute to F_S, whereas high energy and low sediment supply contribute to F_D. Tidal flats with negative values of S are expected to have convex-up profiles and to be more stable, whereas flats with positive values of S lead to concave-up profiles and greater vulnerability to erosion (Mehta et al., 1996; Kirby, 2000, 2002; Mehta, 2002).

3.06.5 Observed Morphology in Response to Tides, Waves, and Sediment Supply

3.06.5.1 Profile Convexity/Concavity as a Function of Tidal Range and Wave Exposure

Several authors have demonstrated observationally that the shape of tidal flats tends to become more convex-up as tidal range increases (Dieckmann et al., 1987; Kirby, 2000; Bearman et al., 2010a; **Figure 20**). Assuming that increased tidal range within a given geographical region is a reasonable proxy for the dominance of tidal energy over wave energy, these observed trends of increasing convexity with increased tidal dominance are generally consistent with the theoretical predictions discussed in the previous sections. To clarify the characteristic shape of topographic profiles over entire tidal flat areas, observations of tidal flat shape are often presented in terms of hypsometry, which is the total wetted surface area of a tidal flat system presented as a function of elevation. Hypsometry provides a measure qualitatively similar to a topographic profile, while allowing locally irregular basin topography to be smoothed by along-shore integration. Dieckmann et al. (1987) presented observations of increasingly convex-up tidal flat hypsometry as a function of increased tidal range along the German Bight (**Figure 20(a)**), whereas Kirby (2000) did the same for tidal flats around the UK (**Figure 20(b)**). In addition, Kirby (2000) also noted a strong connection between increased tidal range and greater percentages of flat area found above mean tide level.

Insight into the morphology of intertidal areas under conditions of strong wave forcing can also be gained from observations of macrotidal beach profiles (**Figure 21**). Masselink and Short (1993) synthesized observations from 19 beaches around Australia with spring tidal ranges between 3.6 and 9.5 m. They found beach profile shape between the upper edge of high-water swash and the lower edge of the low-water surf zone to be largely a function of the dimensionless sediment fall velocity, $\Omega = H_b/(w_s T)$ and the relative tidal

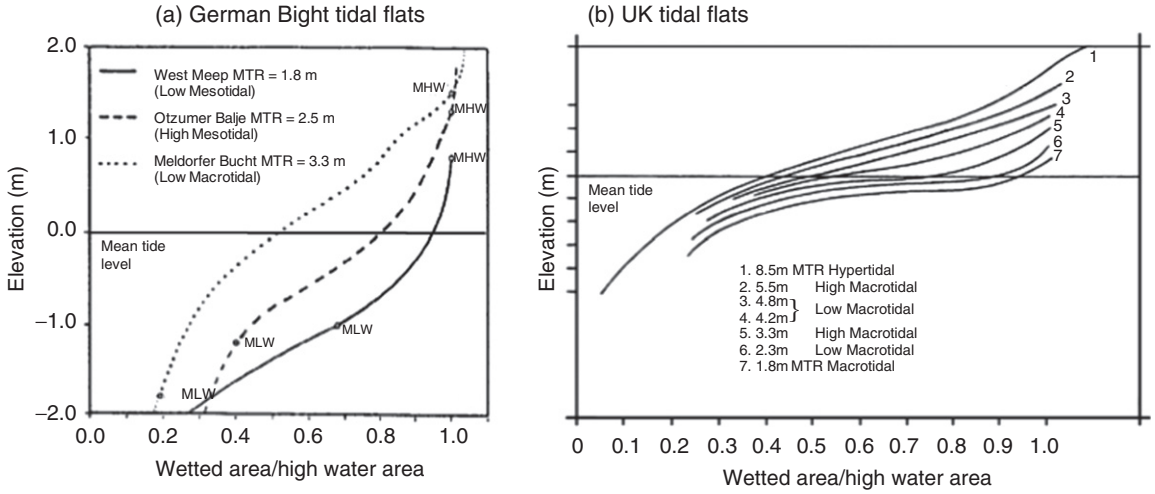

Figure 20 Observations of the total wetted surface area of tidal flat systems as a function of tidal elevation, normalized by the total amounted of wetted surface area at high tide. (a) German Bight tidal flats (Dieckmann et al., 1987), (b) UK tidal flats (Kirby, 2000). Area as a function of elevation, also known as hypsometry, provides a measure qualitatively similar to tidal profile shape, while allowing irregular basin topography to be smoothed by integration. The hypsometry of tidal flats tends to become more convex-up as tidal range increases and more concave-up as tidal range decreases. (a) Modified from Dieckmann, R.M., Osterthun, M., Partenscky, H.W., 1987. Influence of water-level elevation and tidal range on the sedimentation in a German tidal flat area. Progress in Oceanography 18, 151–166. (b) Modified from Kirby, R., 2000. Practical implications of tidal flat shape. Continental Shelf Research 20, 1061–1077.

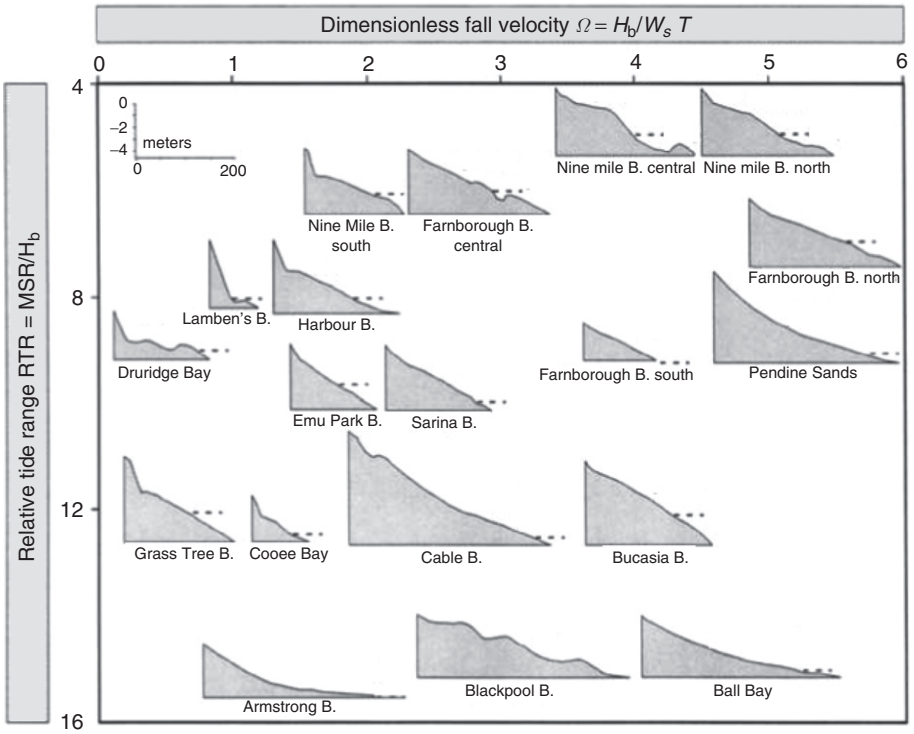

Figure 21 Observed beach profiles as a function of tidal range. Beach profile shape is largely function of dimensionless sediment fall velocity and relative tide range (see text for definition of symbols). As tidal range increases or sediment grain sizes decreases, beach profiles are observed to become wider and less strongly concave-up. Modified from Masselink, G., Short, A.D., 1993. The effect of tide range on beach morphodynamics and morphology: a conceptual beach model. Journal of Coastal Research 9, 785–800.

range (RTR) = MSR/H_b, where H_b is the breaking wave height, w_s the sediment fall velocity, T the wave period, and MSR the mean spring tidal range. They found that increasing tidal range on low wave energy microtidal beaches initially increases concavity through the formation of a low-tide terrace at the base of the more reflective and steeper beach face. As tidal range continues to grow, the beach widens, the dissipative low-tide terrace tilts to encompass more of the tidal range, and the overall beach profile becomes less strongly concave-up. Increasing tidal range on higher energy beaches reduces the dominance of a single classical along-shore bar, favoring a wider, ultra-dissipative and generally less concave topographic profile. Thus, observations of beaches also generally support the concept that increased tidal influence eventually reduces profile concavity.

3.06.5.2 Profile Width and Slope as a Function of Tidal Range and Wave Exposure

Observations of tidal flat width as a function of tidal range under conditions of presumed tidal dominance at first do not seem entirely consistent with simple model predictions from Section 3.06.4. Data from natural tidal flats in **Figure 20** suggest that the intertidal portion of profiles become wider with increased tidal range, whereas 1-D model results suggest that higher range profiles should become steeper without becoming wider (see **Figure 18a**). However, this assumes tidal currents to be oriented entirely cross-shore. On middle-to-lower tidal flats, tidal currents tend to have a strong along-shore component (See **Figure 16(b)**), the strength of which can be expected to increase with tidal range. Tidal currents in channels along the base of a flat would also be expected to become stronger with greater tidal range (Friedrichs, 1995). Stronger along-shore currents mean stronger resuspension and, all else being equal, higher suspended sediment concentrations on the lower flat. Higher concentrations near the seaward boundary then favor wider equilibrium tidal flat widths (cf. **Figure 18(b)**). Higher tidal ranges also generally favor faster rising tides and flood dominance (Friedrichs, 2010); this enhances sediment import, which may further promote higher concentrations and, therefore, wider flats.

Based on observations, the effect of waves on tidal flat width is also somewhat ambiguous. Given that larger tides lead to wider flats in **Figure 20**, one might assume that a smaller tidal range to wave height ratio, R/H, might generally lead to narrower flats. However, the trend at the extreme of tidal beaches is the opposite: a larger R/H ratio leads to wider beach profiles (**Figure 21**). Pethick (1996) found that for mudflats along the Humber estuary, UK, areas with greater wave exposure had wider, concave-up flats, whereas sheltered areas had narrower, convex-up flats (**Figure 22**). A similar, albeit weaker, relationship between overall tidal flat width and wave-induced concavity was reported by Bearman et al. (2010a) for flats fringing South San Francisco Bay. Observed slopes on wave-dominated and/or erosional mudflats are reasonably consistent with the predictions of the F93/FA96 solution shown in **Figure 19**. Profile slopes are between 0.01 and 0.001 over the majority of the intertidal regions of (1) the

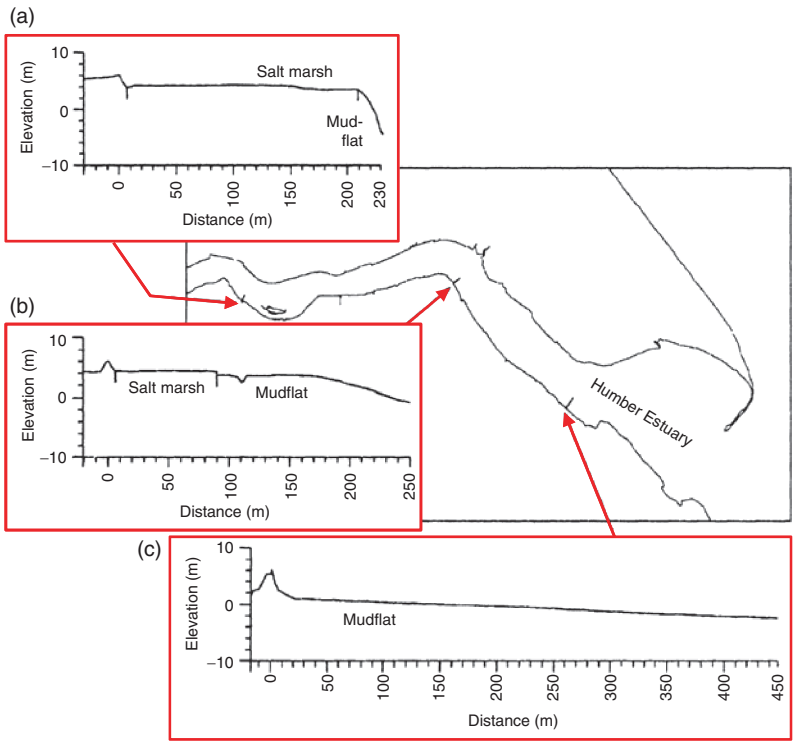

Figure 22 Topographic profiles across tidal marsh and adjacent mudflats along the Humber Estuary, UK. Tidal flats become narrower, steeper, and more convex as one moves upstream along the Humber, away from the more prominent influence of waves near the estuary mouth. Modified from Pethick, J.S., 1996. The geomorphology of mudflats. In: Nordstrom, K.R., Roman, C.T. (Eds.), Estuarine Shores: Evolution, Environments and Human Alterations. Wiley, Chichester, pp. 185–211.

wave-exposed flats near the mouth of the Humber displayed in **Figure 22(c)**, (2) the eroding flats in Jiangsu Province, China, displayed in **Figure 23(c)**, and (3) the eroding profile from Cheniére au Tigre, Louisiana, displayed in **Figure 23(d)**. However it is clear that the overall shapes of these observational cases are not as simple as the idealized profile in **Figure 19**. Pethick (1996) suggested that the width of wave-dominant tidal flats, L, increased as wave height increased because more distance is then required to fully attenuate larger waves. This concept is consistent with the wave-dominated, large R prediction that $L \approx L_w$ based on F93/FA96 (see eqn [7b]), where L_w is the distance over which waves dissipate with U_W capable of disturbing sediment. However, the role of the antecedent geological setting should also be kept in mind. The width of tidal flats in the inner parts of tidal estuaries (where waves become less important) may be constrained simply because the paleo-river valley occupied by the estuary decreases in width landward. Observations of wide energetic beaches with wave height fixed relative to tidal range (Masselink and Short, 1993) also suggest that greater wave energy causes the overall profile to become less steep, in this case as the wave height parameter $\Omega = H_b/(w_s T)$ increases (see **Figure 21**). Widening and flattening with smaller w_s are also consistent with F93/FA96 if smaller settling velocity is considered a proxy for higher local sediment mobility (i.e., lower U_c).

The concave-up shape of wave-dominated flats leads the lower slope portion of the profile to be concentrated at a lower elevation on the overall tidal flat profile (Kirby, 2000) while causing the upper part of the profile to be relatively steep. Therefore, even though the profile-averaged slope decreases with larger waves when approaching the asymptote of complete wave dominance, adding waves to a tidally dominated profile may initially increase the slope of the profile near the high-water line. This may explain why the 1-D time-stepping model of Roberts et al. (2000) for very wide flats with small waves suggested that waves make profiles slightly narrower (see **Figure 18(c)**). Waeles et al. (2004), who included more hydrodynamic mechanisms in their model, found that adding small waves to a very wide tidal flat increased the bed slope near the high-water line, but decreased the bed slope near and below the low-water line.

Le Hir et al. (2000) presented observations of wave height, H, on tidal flats as a function of tidally varying water depth, h, that can be used to help further constrain the validity of the F93/FA96 solution via application of eqn [8]. **Figure 24** displays observations of H versus h for mudflats in Marennes-Oléron Bay and along the Seine Estuary, France. The asymptotic values for H/h of about 0.15–0.3 in **Figure 24** are smaller than classic values for depth-limited breaking and suggest that wave height at these sites is indeed being dissipated mainly by bottom friction. In applying eqn [8], if one uses $f_w \approx 0.1$ and chooses a value of dh/dx halfway along the curve in **Figure 19(b)** (i.e., $dh/dx \approx 0.003$), then the predicted result is $H/h \approx 0.2$, which is reasonably consistent with the observed asymptotic values of H/h in **Figure 24**.

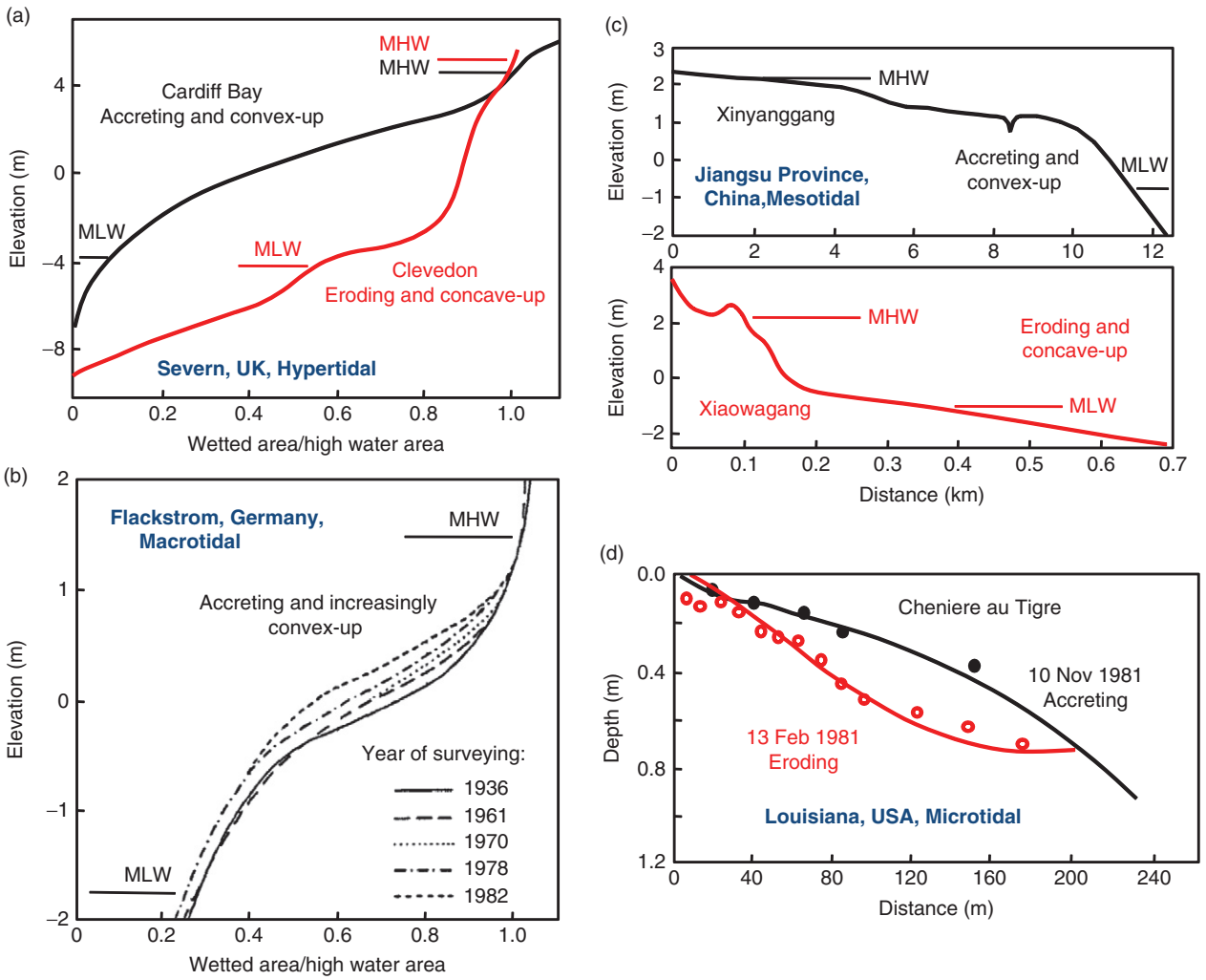

Figure 23 Hypsometry or profiles of accreting vs. eroding tidal flats. (a) Hypertidal flats along the Severn, UK; (b) macrotidal flats from Flackstrom, Germany; (c) mesotidal flats from Jiangsu Province, China; (d) microtidal flats from Cheniere au Tirge, Louisiana, USA. Eroding flats tend to be concave-up, whereas accreting flats tend to be convex-up. (a) Modified from Kirby, R., 1992. Effects of sea level rise on muddy coastal margins. In: Prandle, D. (Ed.), Dynamics and Exchanges in Estuaries and the Coastal Zone. Springer, Berlin, pp. 313–334. (b) Modified from Dieckmann, R.M., Osterthun, M., Partenscky, H.W., 1987. Influence of water-level elevation and tidal range on the sedimentation in a German tidal flat area. Progress in Oceanography 18, 151–166. (c) Modified from Ren, M., 1992. Human impact on coastal landform and sedimentation - the Yellow River example. GeoJournal 28, 443–448. (d) Modified from Woodroffe, C.D., 2002. Coasts: Form, Process and evolution. Cambridge University Press, Cambridge, 640 pp.

A somewhat smaller H/h at the Marennes-Oléron flats than at the Seine flats is furthermore consistent with the presence of a gentler bed slope at Marennes-Oléron (Le Hir et al., 2000). The F93/FA96 equilibrium solution predicts that only one value of H should apply at any given point across a wave-dominated flat because F93/FA96 applies specifically at high water. However, the values of H and h in **Figure 24** span the entire tidal cycle. For stages of the tide below high water, the entire F93/FA96 calculation can qualitatively be thought of as shifting seaward such that wave orbital velocities reach U_c and begin to strongly dissipate energy further seaward, leading to smaller values of H on the flat itself. The fact that H (and, therefore, U_W) is largest at high water in **Figure 24** generally supports the F93/FA96 assumption that high water is most important for overall wave-induced mobilization of the seabed, at least on the middle to upper flats.

3.06.5.3 Depositional versus Erosional Flats

Numerous authors have noted that accretionary flats tend to be convex-up, whereas erosional flats tend to be concave-up (Mehta et al., 1996; Dyer, 1998; Van Rijn, 1998; Kirby, 2000, 2002; Le Hir et al., 2000; Mehta, 2002; Bearman et al., 2010a, 2010b). This tendency holds consistently across a broad spectrum of tidal ranges including, for example, hypertidal flats along the Severn (**Figure 23(a)**; Kirby, 1992), low-macrotidal flats in the German Bight (**Figure 23(b)**; Dieckmann et al., 1987), low-mesotidal flats in Jiangsu Province (**Figure 23(c)**; Ren, 1992), and microtidal flats along the Gulf of Mexico (**Figure 23(d)**; Lee and Mehta, 1997; Woodroffe, 2002). As discussed in Section 3.06.2.3, onshore transport and deposition on flats tend to be associated with dominance by tidally induced energy gradients, whereas offshore transport and

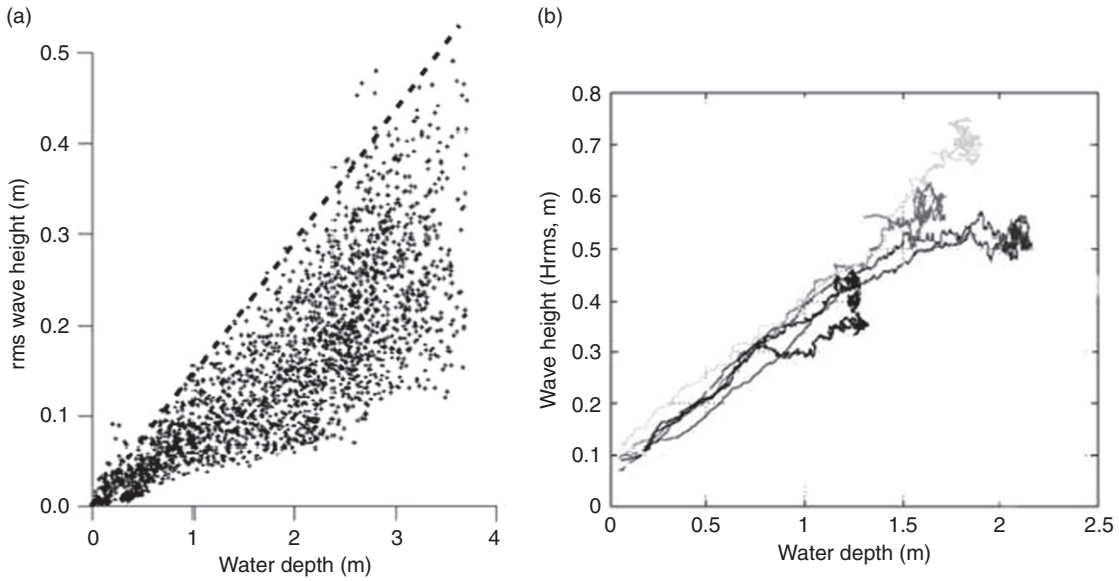

Figure 24 Observed root mean square wave height versus water depth for (a) the Brouage mudflat, Marennes-Oléron Bay, France, from 20 days in October 1994 (o) and 9 days in November 1997 (+) and (b) the Northern mudflat of the Seine estuary, France, from a single storm, 12–14 February 1997. The dashed line in (a) is $H = 0.15$ h. Such a low proportionality between H and h is consistent with dissipation by bottom friction. Observations are also consistent with largest U_W occurring near high tide. Reproduced from Le Hir, P., Roberts, W., Cazaillet, O., Christie, M., Bassoullet, P., Bacher, C., 2000. Characterization of intertidal flat hydrodynamics. Continental Shelf Research 20, 1433–1459.

erosion tend to be associated with dominance by wave-induced energy gradients. Thus, the association of convex-up profiles with both accretion and tidal dominance makes sense, as does the association of concave-up profiles with both erosion and wave dominance.

It could be argued that generic deposition on a tidal flat by almost any process should lead to greater convexity, whereas erosion by almost any means should lead to greater concavity. Enhanced mudflat deposition due to summertime bioaggregation and adhesion in the conceptual model of Andersen et al. (2005) seasonally increases profile convexity, for example (see **Figure 10**). However, this trend will only strictly be the case if erosion or deposition is centered on the middle portion of the tidal flat. If topographic change were focused instead at the extremes of tidal elevation, then deposition would instead increase concavity, and erosion would increase convexity. It is thus an important finding that waves and tides cause erosional flats to be concave-up and depositional flats to be convex-up.

3.06.5.4 Combined Effects of Tides, Waves and Recent Erosion or Deposition

The morphodynamic discussion to this point clearly supports the conclusion that small waves, large tides, and sediment import all favor a convex-up tidal flat profile, whereas large waves, small tides, and sediment export all favor a concave profile (cf. Kirby, 2000). As waves, tides, and sediment supply effects all occur together, it can be difficult to use observations to separate these influences on equilibrium morphology. A technique that is promising in this regard is the use of eigenfunction analysis to identify dominant components of profile variability within large data sets. Bearman et al. (2010a) applied eigenfunction analysis to ~700 tidal flat profiles distributed across 12 zones around the edge of South San Francisco Bay (**Figure 25(a)** and 25(**b**)). The 12 zones were chosen to represent distinct morphodynamic regions, separated from each other by promontories or the mouths of major tidal creeks (**Figure 25(b)**). Once the 700 profiles were normalized with respect to profile length (which everywhere extended from mean high water to 0.5 m below mean low water), the first eigenfunction explained 90% of the variance in profile elevation away from the overall mean profile (**Figure 25(c)**). In other words, the first eigenfunction times the spatially distributed series of eigenfunction scores, when added to the mean profile, explained nearly all aspects of tidal flat profile shape around South San Francisco Bay. Profiles with positive eigenfunction scores were more convex-up, whereas those with negative scores were more concave-up (**Figure 25(d)**).

Bearman et al. (2010a) then compared regionally averaged eigenfunction scores around South San Francisco Bay to regionally representative parameters for tides, waves, and recent thicknesses of deposition or erosion, and found significant correlations among these factors and the resulting morphology (**Figure 26**). Consistent with the discussion throughout this chapter, greater tidal ranges, smaller waves (as represented by shorter fetch), and net deposition were all significantly correlated with greater convexity (i.e., positive scores), whereas smaller tidal ranges, larger waves, and net erosion were all significantly correlated with greater concavity (i.e., negative scores). Furthermore, a multiple regression of tidal range, wave fetch, and net deposition against observed scores allowed Bearman et al. (2010a) to examine the combined influence of these three factors in order to statistically rank their relative importance. This suggested that the most important factor governing present profile shape was (1) degree of recent deposition or erosion, followed by (2) local tidal range, and

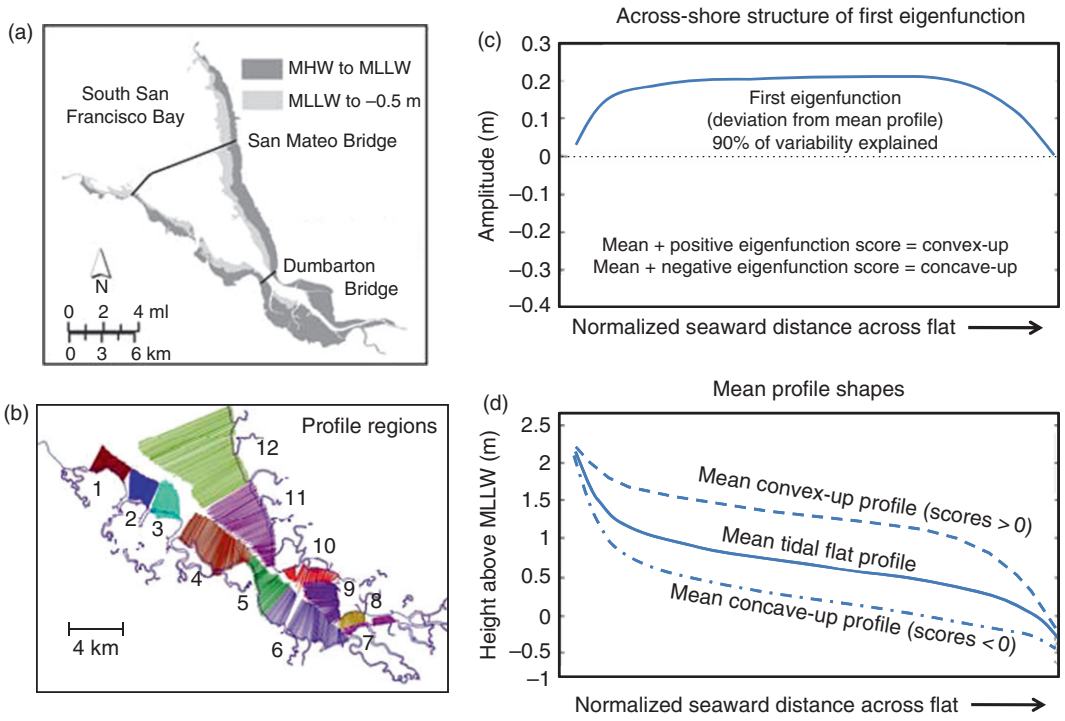

Figure 25 Eigenfunction analysis of tidal flat morphology in South San Francisco Bay. (a) Distribution of flat areas between mean high water (MHW), mean lower low water (MLLW), and 0.5 m below MLLW; (b) distribution of 700 topographic profiles within 12 morphological regions; (c) structure of first eigenfunction, which explains 90% of the profile variance around the mean; (d) mean of all profiles and mean of profiles with positive (or negative) scores for first eigenfunction. Positive or negative scores correspond to convex-up or concave-up profiles, respectively. Modified from Bearman, J.A., Friedrichs, C.T., Jaffe, B.E., Foxgrover, A.C., 2010a. Spatial trends in tidal flat shape and associated environmental parameters in South San Francisco Bay. Journal of Coastal Research 26, 342–349.

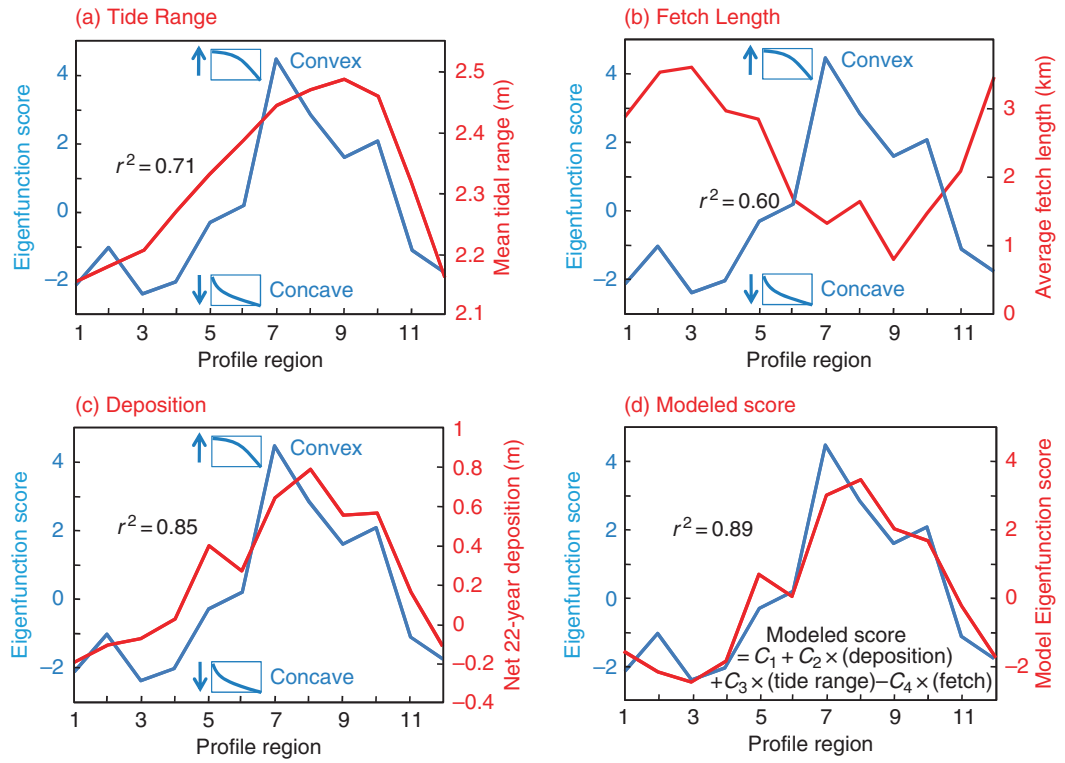

Figure 26 Comparison of average eigenfunction scores for profile shape in 12 regions around South San Francisco Bay (>0 = convex-up, < 0 = concave-up) to (a) local mean tidal range, (b) average local fetch length, (c) net deposition (>0) or erosion (< 0) between 1983 and 2005, and (d) best-fit modeled score determined by a multiple linear regression of (a)–(c) against observed score. The strongest predictor of profile shape is past deposition/erosion, followed by tidal range and then wave fetch. Modified from Bearman, J.A., Friedrichs, C.T., Jaffe, B.E., Foxgrover, A.C., 2010a. Spatial trends in tidal flat shape and associated environmental parameters in South San Francisco Bay. Journal of Coastal Research 26, 342–349.

finally (3) wave height as parametrized by fetch length. The multiple regression model forced by tides, waves and past deposition/erosion accounted for 89% of the spatial variability in the regionally averaged eigenfunction scores (**Figure 26(d)**).

3.06.6 Extreme Timescales of Change: From Sea Level to Grain Size Patterns

3.06.6.1 Timescales of Change

As pointed out by Pethick (1996), the rate of response of the large-scale morphology of tidal flats to changing wave or tidal forcing is much slower than the morphodynamic response of sandy beaches. This is due to the generally larger cross-shore extent of flats as well as their typically lower energy relative to beaches. The modeling results of Pritchard et al. (2002) (see **Figure 15(c)**) suggest that it takes several years in the presence of $\sim 1\,g\,l^{-1}$ of suspended sediment at a flat's seaward boundary for a tidal flat profile to adjust vertically on the order of a meter in the presence of steady-state, relatively strong tidal currents. This means that natural tidal flats rarely reach a static equilibrium in response to the seasonally evolving tide and wave forcing to which they are typically exposed. The predicted equilibria for tidal dominance and wave dominance are so different from each other, and a single season is too short a time, to reach equilibrium with one extreme forcing or the other. This is in contrast to beaches, for which the hysteresis of morphodynamic adjustment is relatively short, such that the shape of beach profiles can usually fully reach a state of equilibrium in response to a given set of wave and tide forcing (e.g., Masselink and Short, 1993; Woodroffe, 2002). **Figure 27** documents a typically slow response of tidal flat slope on the Dengie Peninsula, UK, to seasonally changing wave energy relative to more seasonally uniform tidal energy (Pethick, 1996).

During calm weather, the slope of the Dengie flats continually increases until the onset of winter storms. The slope then decreases incrementally in response to each storm (although individual storms are not resolved in **Figure 27**), until the tidally dominated recovery period begins once more. The morphological response of the tidal flats neither during the stormy season nor during the calm season shows any indication of slowing with time or of approaching a static equilibrium (**Figure 27**). Although the morphologic adjustment during an individual storm is likely to proceed much more quickly than the cycle of recovery during calm weather, waves on tidal flats are rarely intense or persistent enough to reach a static wave-dominated equilibrium during a single season. The presence of a similar, iteratively evolving intermediate state is also implied for the wave- and tide-impacted flats in **Figures 7**b and **8**. These case studies indicate that for both the Severn flats in the UK and the Yangtze River mouth flats in China, tidal flat erosion occurs incrementally in response to each storm, and deposition occurs continually under tidal dominance. But neither storm nor tidal dominance is persistent enough to create a static equilibrium. Nonetheless, an individual system's average morphological form is expected to remain relatively unchanged from year to year, since over the long term, the seasonal effects of tide- and wave-induced deviations from the long-term profile shape nearly cancel out. Thus, we can still consider the annual average morphology to represent a type of dynamic equilibrium with the combined effects of both waves and tides.

Although the large-scale morphodynamic adjustment of tidal flats is generally slower than seasonal fluctuations in wave versus tidal energy, the morphodynamic adjustment of tidal flats is still fast in comparison to the century-plus timescale of relative sea-level rise, the decade-plus scales of most engineering works, and other decade-plus changes in sediment supply, wave climate, or tidal forcing. The decadal-scale adjustment of the Flackstrom tidal flat illustrated in **Figure 23(b)** was hypothesized by Dieckmann et al. (1987) to be in response to plentiful sediment supply in combination with the 0.3-m increase in both mean water-level and mean tidal range that had occurred gradually in the region over the last 100 years.

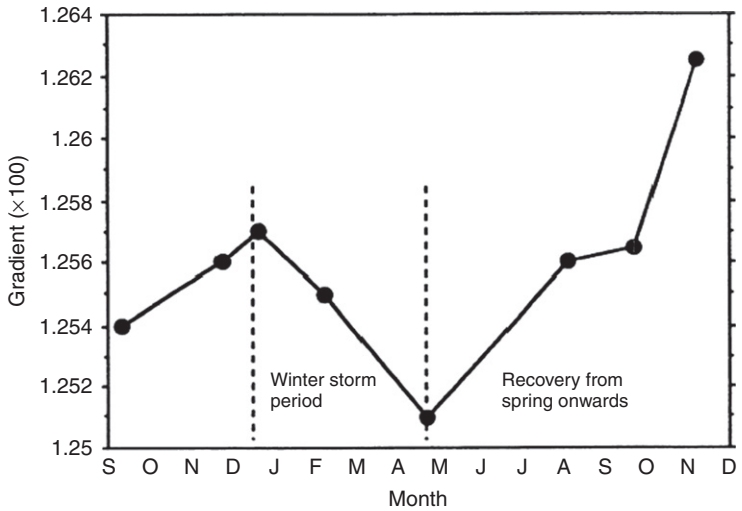

Figure 27 Response of the slope of a muddy tidal flat to seasonal cycles of tide- and wave-dominated forcing on the Dengie Peninsula, UK. Neither the decrease in slope in response to a series of storms nor the increase in slope during recovery under tidal forcing shows any indication of slowing with time or approaching a static equilibrium. Reproduced from Pethick, J.S., 1996. The geomorphology of mudflats. In: Nordstrom, K.R., Roman, C.T. (Eds.), Estuarine Shores: Evolution, Environments and Human Alterations. Wiley, Chichester, pp. 185–211.

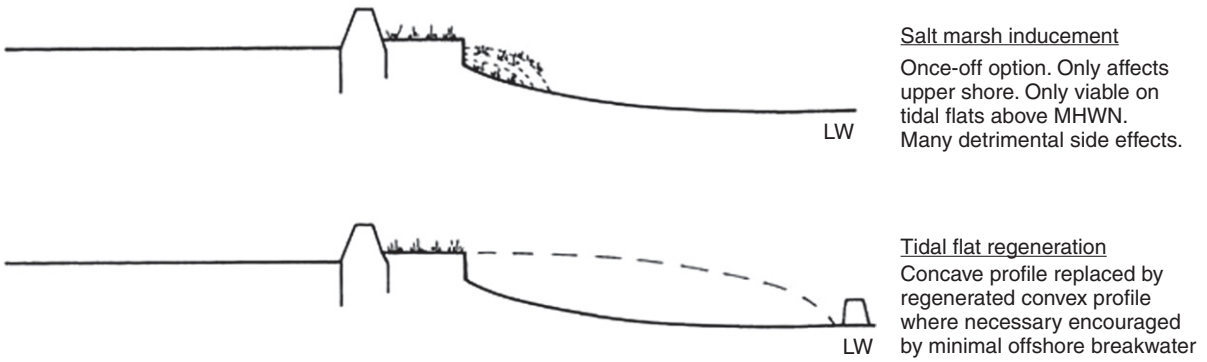

Figure 28 Diagrammatic cross-sectional representation of sediment engineering options along an eroding muddy coastline backed by a seawall. (a) Constructing an additional marsh near the high-water line (MHWN = mean high water neap), (b) placing a breakwater near the low-water (LW) line and backfilling with dredge material. Constructing a marsh over-steepens the concave-up tidal flat profile beyond its previous erosional equilibrium shape, possibly accelerating erosion further. A breakwater that reduces wave energy may allow for a convex depositional equilibrium shape to remain more stable, mitigating the previous erosional tendencies. Modified from Kirby, R., 2000. Practical implications of tidal flat shape. Continental Shelf Research 20, 1061–1077.

Since Pritchard et al. (2002) (see **Figure 15(c)**) found that a tidal flat could easily adjust by ~1 m in elevation over a decade, it is unlikely that there is a notable time lag in the ~10 cm per decade morphodynamic response of the Flackstrom flat. In their study of the evolution of the shape of tidal flat profiles in South San Francisco Bay from the 1890s to 2005, Bearman et al. (2010b) correlated decade-plus changes in profile convexity/concavity to decade-plus changes in riverine sediment supply without needing to incorporate a time lag either. Given the rapid adjustment of tidal flat morphodynamics relative to engineering time scales, Kirby (2000) suggested that human-imposed reductions of overall wave energy offshore of tidal flats could be a viable option for tidal flat regeneration (**Figure 28**). Placement of an offshore breakwater in combination with back-filling may create a new stable convex shape in dynamic equilibrium (over annual time scales) with the now lower-energy wave climate. By contrast, rebuilding the salt marsh alone might exacerbate the problem by further steeping the tidal flat beyond its previous erosional state, thus accelerating the erosional translation of the profile even faster than before.

3.06.6.2 Mean Grain-Size Patterns

Surficial grain size on tidal flats can significantly respond to spatial gradients in energy much more quickly (e.g., during a single storm) than the overall profile shape can fundamentally adjust (which requires years). Thus, it follows that the classic fining of grain size toward the high-water line across tidal flats may be usefully interpreted as a lowest-order response to persistent short-term morphological disequilibrium. Although the mean shape of most tidal flats is in a near dynamic equilibrium when considered over an annual cycle, most profiles are instantaneously out of equilibrium with forcing over individual tidal cycles or storms. The slope of natural tidal flats intermittently exposed to waves is almost never sufficiently convex to prevent a decrease in energy toward shore under tides alone; likewise, the slope is almost never sufficiently dissipative to prevent an increase in energy toward the shore during occasional periods of large waves. As the majority of the time most tidal flats are mainly under the influence of tides rather than waves, it follows that most of the time there is a broad pattern of sediment fining toward the high-water line, consistent with the usual tidal energy gradient. Yet, the overall morphology cannot fully evolve to reach a static equilibrium with the usual tidal forcing. This is because shorter events with stronger waves so effectively readjust the incremental morphological change that has previously occurred under longer periods of slow but steady tidal dominance.

The general pattern of coarser sediments in channels and on lower flats grading to finer sediment on upper flats is found in the majority of tidal flat systems (see **Figure 1**), although the range and centroid of the grain-size spectrum depend on the overall energy level and on the size and supply of externally available source material (e.g., Mai and Bartholomä, 2000). For example, higher-energy, open-coast flats tend to be sandier, whereas sheltered estuarine and back-barrier flats tend to be muddier (see **Figure 1**). For South San Francisco Bay, Bearman et al. (2010a) found that concave, more erosional flats exhibited overall coarser grain sizes than convex, more depositional flats. **Figure 29** displays a typical spatial pattern of tidal flat grain sizes, with fine sand near the low-water line grading to mud near the high-water line (Gadow, 1970). This example from Jade Bay in Germany clearly demonstrates how closely tied surficial grain size can be to spatial patterns of peak tidal velocity (Grabemann et al., 2004). However, local reversals in the typical grain-size gradient across tidal flats can occur in association with localized input of terrestrial runoff or in response to persistent wave breaking at a given topographic contour. The availability of mud can also play an important role in determining the dominant grain size. High supply contributes to extensive mudflats being present along open coasts near the mouths of muddy tidal rivers, despite high coastal energy (Amos, 1995). All else being equal, Amos (1995) suggested that sandy flats dominate where the sediment concentration of inundating water is less than ~1 $g\,l^{-1}$, while muddy flats dominate for inundating water with concentrations greater than about ~1 $g\,l^{-1}$.

Across many tidal flats, the distribution of grain sizes in the absence of significant waves can be directly related to the competence of peak tidal flows at each location to

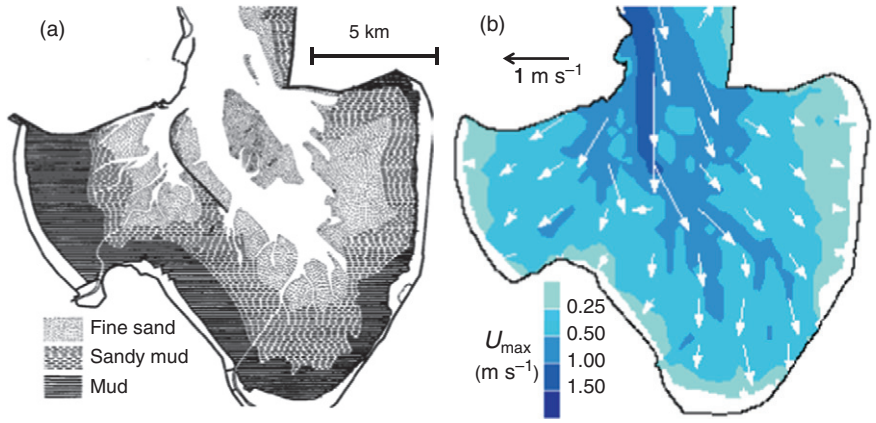

Figure 29 Spatial distribution in Jade Bay, Germany, of (a) surficial sediment grain size and (b) maximum flood tide currents. Surficial grain size in Jade Bay is closely tied to spatial patterns of peak tidal velocity. (a) Modified from Gadow, S., 1970. Sedimente und chemismus. In: Reineck, H.E., (Ed.), Das Watt, Ablagerungs- und Lebensraum, pp. 23–35, Waldemar Kramer, Frankfurt, pp. 23–35. (b) Modified from Grabemann, H.J., Grabemann, I., Eppel, D.P., 2004. Climate change and hydrodynamic impact in the Jade-Weser area: a case study. Coastline Reports 1, 83–91.

suspend sand or erode mud (Amos, 1995). On the tidal flats of both the Wash, UK, and Minas Basin, Canada, the spatial transition from mudflats to sand flats occurs close to the point where peak tidal stress first exceeds the erosion threshold for intertidally exposed muds, that is, ~0.5 Pa (**Figure 30**; Amos, 1995). Because of lag effects, mud can easily be transported to any part of the flat. But cohesion prevents it from being removed once more at locations where tides produce stresses less than ~0.5 Pa. According to Amos (1995), the critical stress for suspension is key to limiting the maximum sand size on the neighboring sand flat. Only fine to medium sand is found in abundance on the sand flats of the Wash and Minas Basin because anything coarser would only be subject to bedload (**Figure 30**). According to Amos (1995) bedload is not sufficient to place coarser sand on the sand flat because suspension is needed to move sand up the steep landward flank of the low-water tidal channel.

3.06.6.3 Time-Varying Grain-Size Patterns

Observations of time-varying sediment texture on tidal flats demonstrate how rapid and significant the change in grain size can be in response to temporal changes in the degree of wave versus tidal forcing. Observations from the Luchaogang open-coast tidal flats near the mouth of the Yangtze River

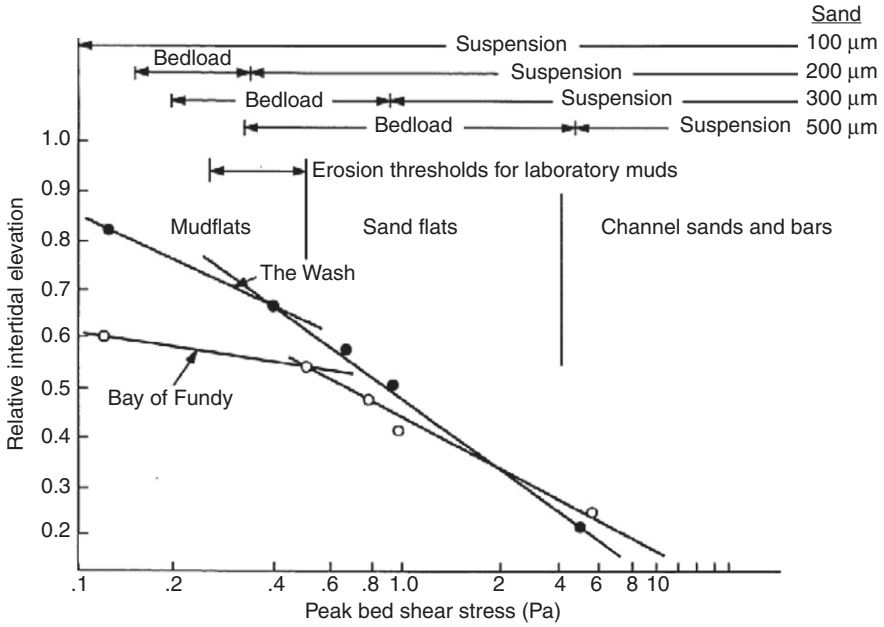

Figure 30 Comparison between peak bed shear stresses and the location of the mud–sand transition across the tidal flats of the Wash, UK, and Minas Basin in the Bay of Fundy, Canada. Also shown in the figure are the range of thresholds for erosion of laboratory muds., and the modes of transport (no motion, bedload, or suspension) of very fine (100 μm) to medium-to-coarse (500 μm) sands. In each case, the mudflats extend to near the laboratory mud erosion threshold, and only sands that can be fully suspended are found on the sand flat. Modified from Amos, C.L., 1995. Siliclastic tidal flats. In: Perillo, G.M.E. (Ed.), Geomorphology and Sedimentology of Estuaries. Elsevier, Amsterdam, pp. 273–306.

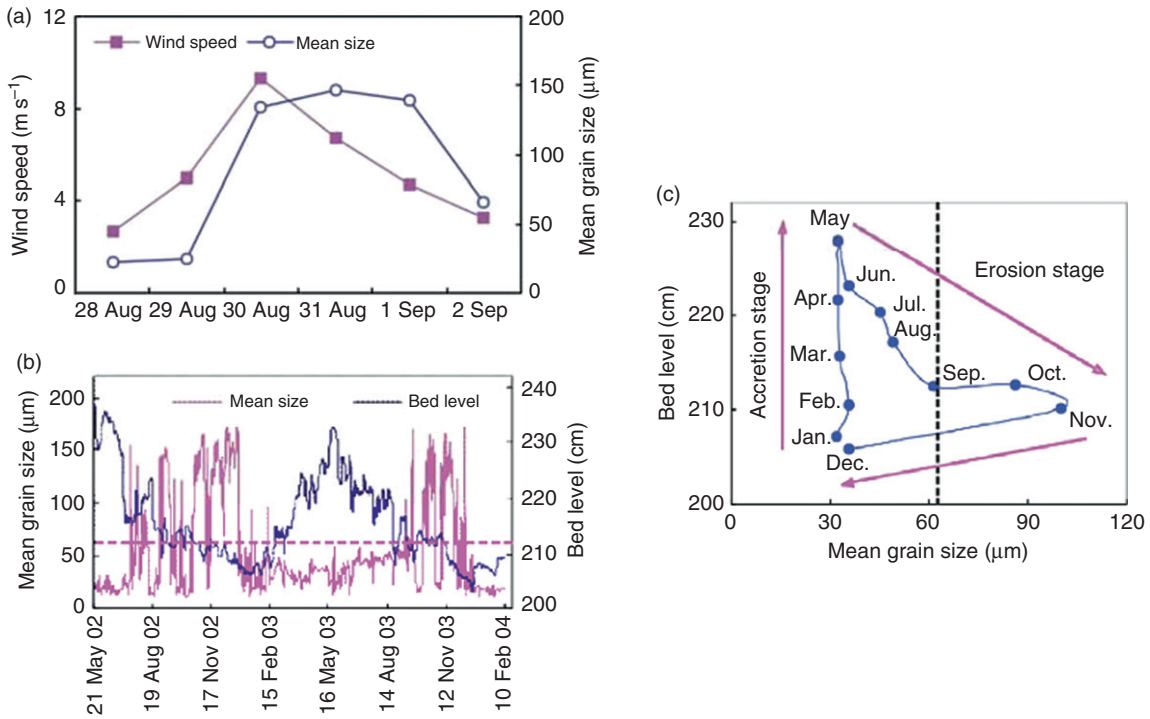

Figure 31 Time series from the middle section of the Luchaogang tidal flat, Yangtze Delta, China. (a) Daily mean grain size of surface sediment and daily mean wind speed from 28 August to 2 September 2002; (b) daily mean grain size and level of the sediment surface (above lowest astronomical tide) from 2002 to 2004; (c) relationship between monthly mean grain size and bed level for 2003. Rapid and significant change in grain size occurs in response to temporal changes in the degree of wave vs. tidal forcing. Modified from Yang, S.L., Li, H., Ysebaert, T., Bouma, T.J., Zhang, W.X., Wang, Y.Y., Li, P., Li, M., Ding, P.X., 2008. Spatial and temporal variations in sediment grain size in tidal wetlands, Yangtze delta: on the role of physical and biotic controls. Estuarine, Coastal and Shelf Science 77, 657–671.

indicate that in response to a single moderately strong wind and wave event, it is possible for the mean surficial grain size on the middle section of a tidal flat to change from 20-μm mud to 130-μm sand within a single day (Yang et al., 2008; **Figure 31(a)**). As winds subside, the tidal action may return a coating of mud once more within only a few more days. When waves systematically change on a seasonal basis, then seasonal shifts in sediment grain size can be expected. On the Luchaogang tidal flats, predominately offshore-directed winds during winter and spring reduce the local wave heights, and a 25-cm thick layer of mud builds up on the middle flats over a course of 4 months (Yang et al., 2008; **Figure 31(b)**). When the winds turn back onshore over the summer and fall, the mud layer begins to erode and the bed coarsens. The fining at the beginning of winter is sudden, but the coarsening is gradual (**Figure 31(c)**), suggesting mud is being mixed somewhat into the bed and then winnowed during wave events. The extreme change in grain size (daily averages vary by up to a factor of 8) relative to the modest changes in bed elevation (an annual excursion of ~25 cm out of a 3.5-m spring tidal range) reinforces the rapidity with which grain size can adjust to hydrodynamic forcing relative to the rate at which overall flat morphology can adjust.

Temporal fluctuations in sediment supply can also systematically change the distribution of surficial grain size across tidal flats. The tidal flats along the south coast of Ganghwa Island, Korea, receive an input of mud each summer in association with monsoon-driven peaks in discharge from the Han River, which has distributary branches flowing along both the east and west sides of the island. The seasonal mud is introduced to the flats from the low-water tidal channel fringing the flat (as opposed to direct runoff from Ganghwa Island), and by August mud to muddy-sand covers the majority of the flats (Chun, 2007; **Figure 32**). After the 1–2-month monsoon has ended, the mud is winnowed from the lower to middle flats, while a fraction of the mud continues to migrate toward the inner flats. After the extent of the inner-flat mud peaks in late fall, mud is eroded from the inner flats as well (Chun, 2007). Superimposed on this seasonal pattern is a systematic along-shore increase in overall mud content and in the offshore position of the mud–sand transition (**Figure 32**) associated with a west-to-east decrease in exposure to waves coming in from the Yellow Sea. Although the results discussed here with regard to grain-size distributions support the idea that forcing conditions change too quickly for most flats to reach an asymptotic convex or concave profile, they also support an association of wave dominance with coarser sediment and tide dominance with finer sediment. Thus, it is reasonable to conclude that convex-up profiles tend to be generally muddier, while concave-up profiles tend to be sandier.

3.06.7 Summary and Conclusions

Tidal flats commonly occur along coasts where the tidal range is large relative to typical wave height. They can be found where hydrodynamic energy is high or low, where sediments are

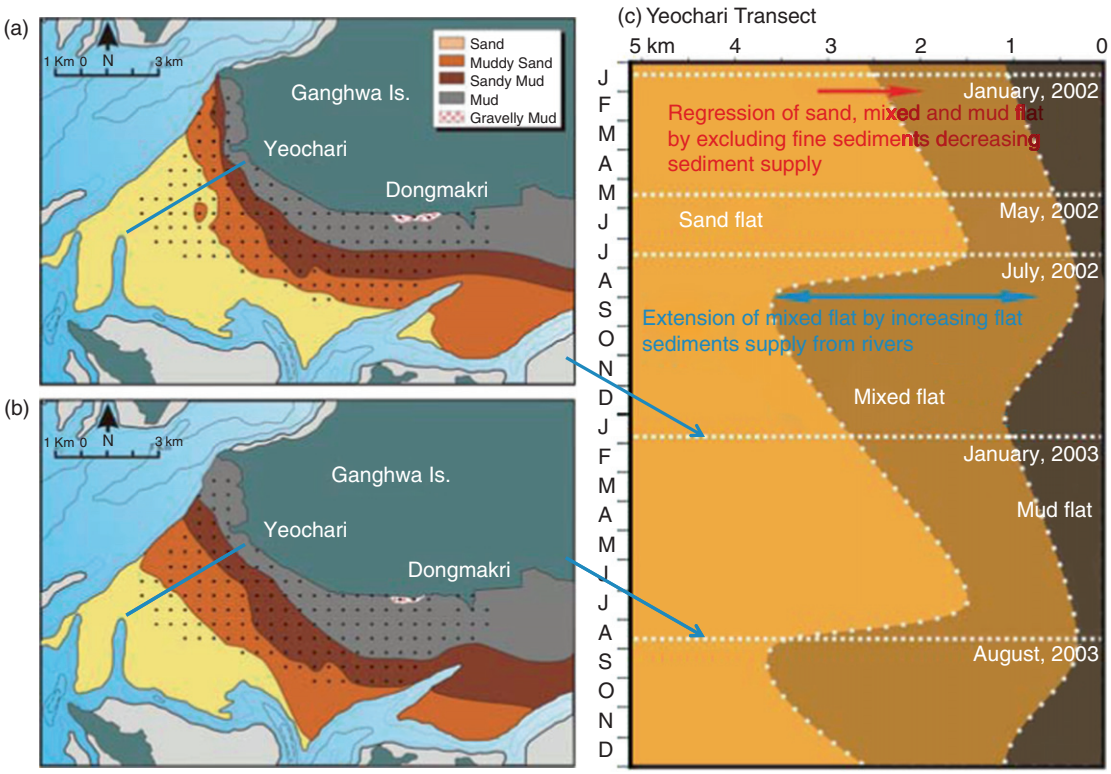

Figure 32 Seasonal change in the spatial distribution of grain size across the south Ganghwa Island tidal flats, Korea. (a) January 2003, (b) August 2003, (c) grain-size distribution along the Yeochari transect from January 2002 through December 2003. On a seasonally averaged basis, the grain-size distribution responds more strongly to the introduction of mud from the Han River than to fluctuations in wave vs. tidal energy. Modified from Chun, S.S., 2007. Sedimentological characteristics of southern intertidal flat of Ganghwa Island, Gyonggi Bay, western coast of Korea. US Office of Naval Research Tidal Flats DRI Planning Meeting, Honolulu, HI, 5-8 June.

sandy or muddy, and where shorelines are prograding, retreating, or stable. The study of the morphology and evolution of tidal flats is particularly well suited in the context of morphodynamics since characteristics such as profile shape, bed slope, and grain size clearly and systematically vary as a function of sediment supply and wave and tidal forcing, and the nature of wave- and tide-induced velocities across tidal flats is, in turn, a direct function of the flat morphology itself.

In this chapter, a tidal flat profile in dynamic equilibrium has been defined as one where its shape remains more or less constant over some characteristic period of natural forcing. The concept of a dynamic equilibrium is a central point of this work. When considered as an average over a typical annual cycle (and when accounting for antecedent geology and anthropogenic effects), this chapter proposes that most tidal flats are characterized by predictable morphologies that are in an approximate dynamic equilibrium with their local climate of waves, tides, and sediment sources and sinks. This does not mean that they are static in space as they are more often than not in the process of advancing or retreating. Rather, it means that when averaged over annual timescales or longer, their characteristic shape and the spatial distribution of surficial grain sizes remain relatively fixed in the reference frame of the flat itself as it recedes or progrades.

Some of the most important concepts, processes, and properties associated with a better understanding of the morphodynamics and dynamic equilibria of tidal flats include the following:

1. It is useful to divide the asymmetries, which drive net sediment transport across tidal flats, into local (Eulerian) asymmetries and spatial (Lagrangian) asymmetries. Eulerian asymmetries involve ebb–flood or high–low water distortion of local tidal velocity. Lagrangian asymmetries follow a periodic excursion of water in space and require (a) horizontal gradients in suspended sediment concentration and (b) a lag in the response of the concentration to bed stress.
2. Simple theory and observations both support the conclusion that tide- and wave-induced bed stresses typically decrease and increase, respectively, with landward distance across tidal flats (**Figure 33**). These two opposite patterns of Lagrangian asymmetry, in turn, drive an analogous landward decrease or increase in peak suspended sediment concentration. Periodic advection then leads to net landward or seaward sediment transport, respectively.
3. Sediment sources and/or sinks can also drive spatial gradients in concentration, which ultimately lead to net sediment transport. Examples include a high sediment concentration boundary condition provided by a tidal river, spatial gradients in the critical stress necessary for sediment resuspension, and/or gradients in settling flux. Common causes of spatial gradients in erodibility and settling include

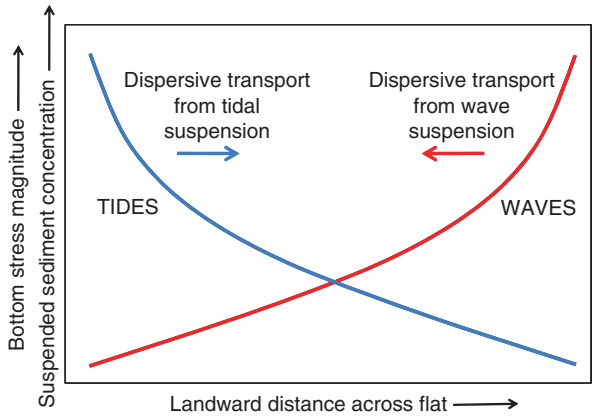

Figure 33 Conceptual diagram summarizing typical patterns of bottom stress magnitude and suspended sediment concentration in response to waves and tides as a function of landward distance across a tidal flat. In each case, sediment is dispersed from areas of higher stress and concentration towards areas of lower stress and concentration.

biological activity and recent deposition of weakly consolidated mud.

4. For flats exhibiting minimal spatial gradients in velocity, stress, or concentration, net sediment transport can still occur over a tidal cycle in response to Eulerian (i.e., local, time-dependent) asymmetries. Coarser sediment is more sensitive to local asymmetries in maximum velocity, whereas fine sediment is more sensitive to local asymmetries in the duration of slack water. Eulerian asymmetries induced by local continuity effects cause tidal velocities, stresses, and concentrations to be greatest near the tidal front, and ebb–flood asymmetry reflects whether the boundary tide is faster rising or faster falling.

5. Over an entire embayment, continuity and momentum, in the context of a finite channel depth, favor flood dominance, a longer high-water slack, and sediment import, whereas, in the context of intertidal storage, they favor ebb dominance, a longer low-water slack, and sediment export. Locally, flood dominance over flats may be increased by bore-like distortion of the incoming tidal wave. Negative feedbacks at the scale of entire embayments may favor a balance between the effects of finite channel depth and intertidal storage such that local tidal asymmetries are minimized.

6. The asymptote for an equilibrium tidal flat profile subject to symmetric forcing of tidal elevation and velocity in the absence of waves is one whose bathymetry minimizes spatial variations in tidal velocity, bed stress, and, therefore, concentration. Analytical solutions and numerical sediment-transport experiments with sinusoidal tidal forcing at the flat's seaward edge produce convex-up equilibrium profiles of across-shore width $L_x \approx (\cos\theta)(\pi/2+1)\, U_c/\omega$, where U_c is a spatially uniform critical stability velocity, ω the tidal frequency, and θ the angle between the maximum tidal velocity and the shoreline.

7. 1-D sediment-transport models predict the equilibrium width of tidally dominated flats to increase with increased offshore concentration, C, because a higher value of U_c is then needed to maintain uniform C across the width of the flat. Assuming a higher tidal range, R, leads to higher offshore C, then a higher R should also require higher U_c and lead to greater equilibrium flat widths under tidal dominance. For embayments as a whole, negative feedback mechanisms suggest that stability will be favored by a spatial extent of tidal flats which minimizes Eulerian asymmetries by balancing finite channel depth and intertidal storage effects.

8. The asymptote for an equilibrium flat subject only to dissipative shallow-water waves at high water, such that wave orbital velocities are uniform in space, is a concave-up profile. The depth of the profile below high water is given theoretically by $h \approx [(4f_w U_c)/(3\pi\, g^{1/2})]^{2/3}(x')^{2/3}$, where f_w is the wave friction factor, x' is the distance offshore, g is the acceleration due to gravity, and U_c is as defined above.

9. The theoretical width of a wave-dominated tidal flat depends on whether R is larger or smaller than $h_0 = (H_0{}^2 g)/(4U_c{}^2)$, where h_0 is the depth at which the offshore wave height H_0 is first able to mobilize sediment by producing an orbital velocity equal to U_c. For small $R \le h_0$, the width of the tidal flat, L, is simply the distance offshore where $h = R$, the width growing with tidal range as R moves further down the $h \sim (x')^{2/3}$ profile. For large $R > h_0$, L is controlled by the distance offshore where $h = h_0$, the width growing with H_0 in order to provide a longer distance over which to dissipate wave energy. In either case, the ratio of wave height to water depth on the inner flats is given by $H/h = (\mathrm{d}h/\mathrm{d}x)(9\pi)/(4f_w)$.

10. 1-D sediment-transport models and empirical engineering models that include both waves and tides predict that the equilibrium profile is initially convex-up in the absence of waves and becomes progressively more concave as wave energy increases. 1-D modeling also indicates that offshore transport by waves provides a mechanism that can potentially balance onshore transport by tides, leading to a profile that remains stationary in space.

11. Several authors have demonstrated observationally that the shape of tidal flats and macrotidal beaches tends to become more convex (or concave) as tidal range increases (or decreases) relative to wave height or in response to significant accretion (or erosion). Eigenfunction analysis can be used with observations of tidal flat morphology to assess the simultaneous affects of tides, waves, and sediment supply.

12. Observations suggest that tidally dominated flats become wider as tidal range increases, a result which is consistent with model predictions assuming that greater tidal range is associated with higher sediment concentrations. Observations of wave-impacted flats along estuaries suggest that wave-dominated flats widen with increased wave energy, implying that larger waves require a larger distance over which to dissipate energy. This trend and explanation are consistent with the wave-dominated analytical solution developed for $R > h_0$ (see summary point 9 above).

13. The magnitude of bed slope (dh/dx) observed on erosional, concave-up mudflats is on the order of 10^{-2}–10^{-3} and is generally consistent with predictions of the strongly dissipative, wave-dominated analytical solution. The maximum values of wave height relative to water depth (H/h) on mudflats are observed to be about 0.15–0.3 and are also consistent with analytical predictions as a function of $\mathrm{d}h/\mathrm{d}x$ and f_w (see summary point 9).

14. Because the time needed for the shape of a tidal flat profile to reach a near-static equilibrium in response to constant external forcing is typically of the order of several years, natural tidal flats rarely reach instantaneous equilibrium in response to seasonally varying tide and wave forcing. Yet, the net seasonal effects of tide- and wave-induced deviations from the long-term profile shape often nearly cancel out. Thus, we can still consider the annual average morphology to represent a type of dynamic equilibrium in response to the combined effects of both waves and tides. By contrast, the morphological response of most tidal flats is rapid relative to the decade-plus timescales of engineering works, climatic fluctuations, and sea-level rise.

15. Surficial grain size on tidal flats responds to gradients in energy much more quickly than the overall profile shape can respond. It therefore follows that the classic fining of grain size toward the high-water line on tidal flats may be usefully interpreted as a lowest-order response to persistent short-term morphologic disequilibrium.

16. Most of the time, tides in the absence of strong waves result in a decrease in energy toward shore, and the grain-size gradient generally reflects the competence of peak tidal flows at each location to remobilize the local sediment. In addition, the broader grain-size spectrum depends on the size and supply of the available source material. As surficial sediment can easily change from mud to sand in response to a single storm, strong temporal and spatial variations in grain size on tidal flats are common.

17. From the above insights, a conceptual model arises for the shape of tidal flat profiles (**Figure 34**), which is largely consistent with, but further extends previous conceptual profile diagrams presented by others (Dyer, 1998; Van Rijn, 1998; Kirby, 2000; Bearman et al., 2010a). The end members for the two basic types of tidal flat profiles are convex- and concave-up. Although a tide- and wave-dominated static equilibrium theoretically exists at each of these extremes, natural tidal flats over annual timescales are typically at an intermediate dynamic equilibrium somewhere between these two extremes.

18. A more convex-up profile is favored in the presence of increased tidal range, decreased wave height, increased external sediment supply, increased bioaggregation/adhesion, forcing by a faster-rising tide, and/or external forcing by a tide with an extended period around high water. Processes and properties associated with evolution toward a convex-up tidal flat include net shoreward sediment transport, increased deposition, a local decrease in the duration of high-water slack, decreased grain size, and a profile form that progrades seaward.

19. A more concave-up profile is favored in the presence of decreased tidal range, increased wave height, decreased external sediment supply, bioturbation/human disturbance, forcing by a faster-falling tide, and/or external forcing by a tide with a shortened period around high water. Processes and properties associated with the evolution toward a concave-up tidal flat include net seaward sediment transport, increased erosion, increased grain size, a local increase in the duration of high-water slack, and a profile form that retreats landward.

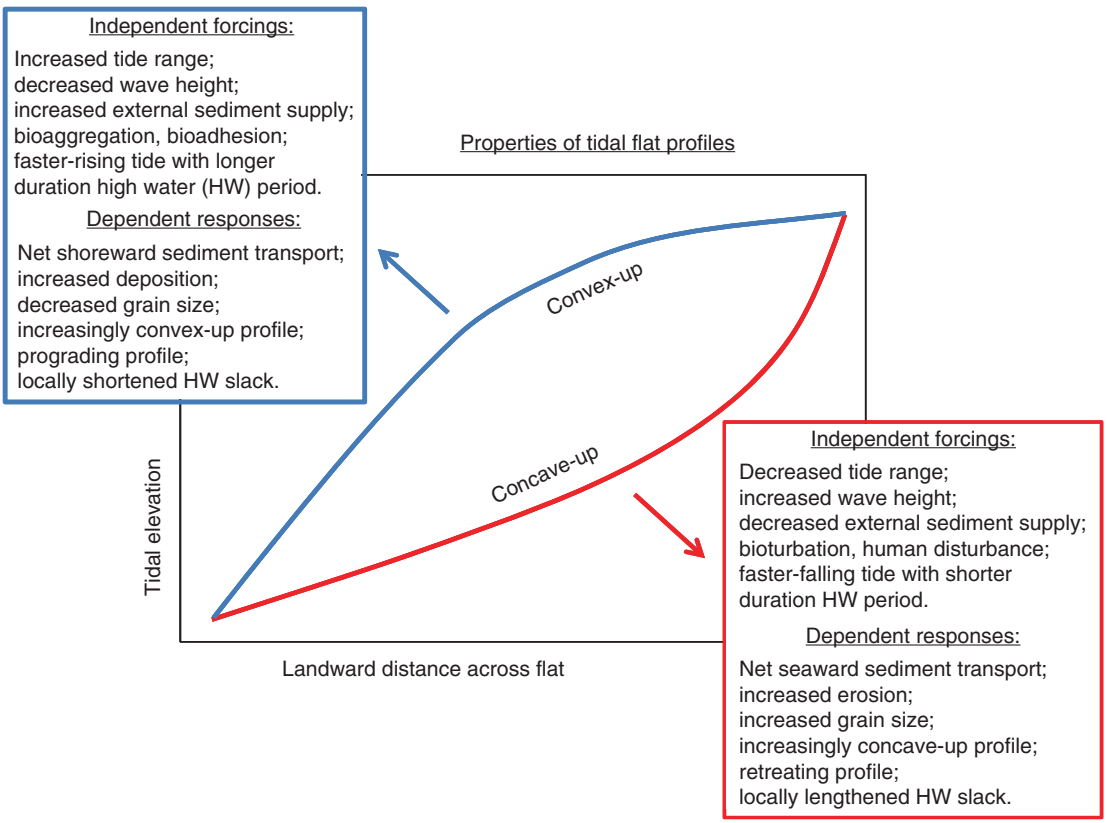

Figure 34 Conceptual diagram summarizing the response of tidal flat shape and properties to a variety of independent forcings favoring either a convex-up or a concave-up profile.

Acknowledgments

Funding for this work was provided by the U.S. Office of Naval Research Coastal Geosciences Program (Grant N00014-07-1-0677) and by the U.S. Geological Survey (Contract Number 06WRSA0285). The author thanks S.S. Chun for generously sharing his recent research findings. This is contribution no. 3154 from the Virginia Institute of Marine Science.

References

Allen, J.R.L., Duffy, M.J., 1998. Medium-term sedimentation on high intertidal mudflats and salt marshes in the Severn estuary, SW Britain: the role of wind and tide. Marine Geology 150, 1–27.

Allison, M.A., Nittrouer, C.A., Kineke, G.C., 1995. Seasonal sediment storage on mudflats adjacent to the Amazon River. Marine Geology 125, 303–328.

Amos, C.L., 1995. Siliclastic tidal flats. In: Perillo, G.M.E. (Ed.), Geomorphology and Sedimentology of Estuaries. Elsevier, Amsterdam, pp. 273–306.

Andersen, T.J., Lund-Hansen, L.C., Pejrup, M., Jensen, K.T., Mouritsen, K.N., 2005. Biologically induced differences in erodibility and aggregation of subtidal and intertidal sediment: a possible cause for seasonal changes in sediment deposition. Journal of Marine Systems 55, 123–138.

Bearman, J.A., Friedrichs, C.T., Jaffe, B.E., Foxgrover, A.C., 2010a. Spatial trends in tidal flat shape and associated environmental parameters in South San Francisco Bay. Journal of Coastal Research 26, 342–349.

Bearman, J.A., Friedrichs, C.T., Jaffe, B.E., Foxgrover, A.C., 2010b. Spatial and temporal trends in tidal flat shape and associated environmental parameters in South San Francisco Bay between the 1890s and 2005. Proceedings of the 15th Physics of Estuaries and Coastal Seas Conference, Colombo, Sri Lanka, 14–17 September.

Boon, J.D., Byrne, R.J., 1981. On basin hypsometry and the morphodynamic response of coastal inlet systems. Marine Geology 40, 27–48.

Chun, S.S., 2007. Sedimentological characteristics of southern intertidal flat of Ganghwa Island, Gyonggi Bay, western coast of Korea. US Office of Naval Research Tidal Flats DRI Planning Meeting, Honolulu, HI, 5–8 June.

Collins, M.B., Ke, X., Gao, S., 1998. Tidally-induced flow structure over intertidal flats. Estuarine Coastal and Shelf Science 46, 233–250.

Cowell, P.J., Thom, B.G., 1994. Morphodynamics of coastal evolution. In: Carter, R.W.G., Woodroffe, C.D. (Eds.), Coastal Evolution, Late Quaternary Shoreline Morphodynamics. Cambridge University Press, Cambridge, pp. 33–86.

Deloffre, J., Lafite, R., Lesueur, P., Lesourd, S., Verney, R., Guézennec, L., 2005. Sedimentary processes on an intertidal mudflat in the upper macrotidal Seine estuary, France. Estuarine Coastal and Shelf Science 64, 710–720.

De Swart, H.E., Zimmerman, J.T.F., 2009. Morphodynamics of tidal inlet systems. Annual Review of Fluid Mechanics 41, 203–229 (plus supplemental material).

Dieckmann, R.M., Osterthun, M., Partenscky, H.W., 1987. Influence of water-level elevation and tidal range on the sedimentation in a German tidal flat area. Progress in Oceanography 18, 151–166.

Dronkers, J., 1986. Tidal asymmetry and estuarine morphology. Netherlands Journal of Sea Research 20, 117–131.

Dyer, K.R., 1998. The typology of intertidal mudflats. In: Black, K.S., Paterson, D.M., Cramp, A. (Eds.), Sedimentary Processes in the Intertidal Zone, Special Publications. Geological Society, London, vol. 139, pp. 11–24.

Dyer, K.R., Christie, M.C., Wright, E.W., 2000. The classification of intertidal mudflats. Continental Shelf Research 20, 1039–1060.

Friedrichs, C.T., 1993. Hydrodynamics and Morphodynamics of Shallow Tidal Channels and Intertidal Flats. Ph.D. Thesis, Massachusetts Institute of Technology/Woods Hole Oceanographic Institution Joint Program, Woods Hole, MA, USA, 218 pp.

Friedrichs, C.T., 1995. Stability shear stress and equilibrium cross-sectional geometry of sheltered tidal channels. Journal of Coastal Research 11, 1062–1074.

Friedrichs, C.T., 2010. Barotropic tides in channelized estuaries. In: Valle-Levinson, A. (Ed.), Contemporary Issues in Estuarine Physics. Cambridge University Press, Cambridge, pp. 27–61.

Friedrichs, C.T., Aubrey, D.G., 1988. Non-linear tidal distortion in shallow well-mixed estuaries: a synthesis. Estuarine Coastal and Shelf Science 27, 521–545.

Friedrichs, C.T., Aubrey, D.G., 1996. Uniform bottom shear stress and equilibrium hypsometry of intertidal flats. In: Pattiaratchi, C. (Ed.), Mixing Processes in Estuaries and Coastal Seas. American Geophysical Union, Washington, DC, pp. 405–429.

Friedrichs, C.T., Cartwright, G.M., Dickhudt, P.J., 2008. Quantifying benthic exchange of fine sediment via continuous, non-invasive measurements of settling velocity and bed erodibility. Oceanography 21 (4), 168–172.

Friedrichs, C.T., Lynch, D.R., Aubrey, D.G., 1992. Velocity asymmetries in frictionally-dominated tidal embayments: longitudinal and lateral variability. In: Prandle, D. (Ed.), Dynamics and Exchanges in Estuaries and the Coastal Zone. American Geophysical Union, Washington, DC, pp. 277–312.

Friedrichs, C.T., Perry, J.E., 2001. Tidal salt marsh morphodynamics: a synthesis. Journal of Coastal Research, SI 27, 3–37.

Friedrichs, C.T., Scully, M.E., 2007. Modeling deposition by wave-supported gravity flows on the Po River delta: from seasonal floods to prograding clinoforms. Continental Shelf Research 27, 322–337.

Friedrichs, C.T., Wright, L.D., 2004. Gravity-driven sediment transport on the continental shelf: implications for equilibrium profiles near river mouths. Coastal Engineering 51, 795–811.

Gadow, S., 1970. Sedimente und chemismus. In: Reineck, H.E., (Ed.), Das Watt, Ablagerungs- und Lebensraum. Waldemar Kramer, Frankfurt, pp. 23–35.

Gao, S., 2009. Geomorphology and sedimentology of tidal flats. In: Perillo, G.M.E., Wolanski, E., Cahoon, D.R., Brinson, M.M. (Eds.), Coastal Wetlands: An Integrated Ecosystem Approach. Elsevier, Amsterdam, pp. 295–316.

Grabemann, H.J., Grabemann, I., Eppel, D.P., 2004. Climate change and hydrodynamic impact in the Jade-Weser area: a case study. Coastline Reports 1, 83–91.

Hayes, M.O., 1979. Barrier island morphology as a function of tidal and wave regime. In: Leatherman, S.P. (Ed.), Barrier Islands from the Gulf of St. Lawrence to the Gulf of Mexico. Academic Press, New York, NY, pp. 1–27.

Janssen-Stelder, B., 2000. The effect of different hydrodynamic conditions on the morphodynamics of a tidal mudflat in the Dutch Wadden Sea. Continental Shelf Research 20, 1461–1478.

Kineke, G.C., Higgins, E.E., Hart, K., Velasco, D., 2006. Fine-sediment transport associated with cold-front passages on the shallow shelf, Gulf of Mexico. Continental Shelf Research 26, 2073–2091.

Kirby, R., 1992. Effects of sea level rise on muddy coastal margins. In: Prandle, D. (Ed.), Dynamics and Exchanges in Estuaries and the Coastal Zone. American Geophysical Union, Washington, DC, pp. 313–334.

Kirby, R., 2000. Practical implications of tidal flat shape. Continental Shelf Research 20, 1061–1077.

Kirby, R., 2002. Distinguishing accretion from erosion-dominated muddy coasts. In: Healy, T., Wang, Y., Healy, J. (Eds.), Muddy Coasts of the World: Processes, Deposits and Function. Elsevier, Amsterdam, pp. 61–81.

Klein, G.D., 1985. Intertidal flats and intertidal sand bodies. In: Davis, R.A. (Ed.), Coastal Sedimentary Environments. Springer, New York, NY, pp. 187–224.

Larson, M., Kraus, N.C., Wise, R.A., 1999. Equilibrium beach profiles under breaking and non-breaking waves. Coastal Engineering 36, 59–85.

Lee, H.J., Jo, H.R., Chu, Y.S., Bahk, K.S., 2004. Sediment transport on macrotidal flats in Garolim Bay, west coast of Korea: significance of wind waves and asymmetry of tidal currents. Continental Shelf Research 24, 821–832.

Lee, S.C., Mehta, A.J., 1997. Problems in characterizing dynamics of mud shore profiles. Journal of Hydraulic Engineering 123, 351–361.

Le Hir, P., Roberts, W., Cazaillet, O., Christie, M., Bassoullet, P., Bacher, C., 2000. Characterization of intertidal flat hydrodynamics. Continental Shelf Research 20, 1433–1459.

Ma, Y., Friedrichs, C.T., Harris, C.K., Wright, L.D., 2010. Deposition by seasonal wave- and current-supported sediment gravity flows interacting with spatially varying bathymetry: Waiapu shelf, New Zealand. Marine Geology 275, 199–211.

Mai, S., Bartholomä, A., 2000. The missing mud flats of the Wadden Sea: a reconstruction of sediments and accommodation space lost in the wake of land reclamation. In: Flemming, B.W., Delafontaine, M.T., Liebezeit, G. (Eds.), Muddy Coast Dynamics and Resource Management. Elsevier, Amsterdam, pp. 257–272.

Masselink, G., Short, A.D., 1993. The effect of tide range on beach morphodynamics and morphology: a conceptual beach model. Journal of Coastal Research 9, 785–800.

Mehta, A.J., 2002. Mudshore dynamics and controls. In: Healy, T., Wang, Y., Healy, J. (Eds.), Muddy Coasts of the World: Processes, Deposits and Function. Elsevier, Amsterdam, pp. 19–60.

Mehta, A.J., Kirby R., Lee, S.C., 1996. Some observations on mudshore dynamics and stability. Report UFL/COEL MP-96/1, University of Florida, Gainesville, FL, USA, 75 pp.

Nielsen, P., 1992. Coastal Bottom Boundary Layers and Sediment Transport. World Scientific, Singapore, 324 pp.

Nichols, M.M., Biggs, R.B., 1985. Estuaries. In: Davis, R.A. (Ed.), Coastal Sedimentary Environments. Springer, New York, NY, pp. 77–186.

Pethick, J.S., 1980. Velocity surges and asymmetry in tidal channels. Estuarine and Coastal Marine Science 11, 331–345.

Pethick, J.S., 1984. An Introduction to Coastal Geomorphology. Arnold, London, 272 pp.

Pethick, J.S., 1996. The geomorphology of mudflats. In: Nordstrom, K.R., Roman, C.T. (Eds.), Estuarine Shores: Evolution, Environments and Human Alterations. Wiley, Chichester, pp. 185–211.

Postma, H., 1961. Transport and accumulation of suspended matter in the Dutch Wadden Sea. Netherlands Journal of Sea Research 1, 148–190.

Pritchard, D., 2005. Suspended sediment transport along an idealised tidal embayment: settling lag, residual transport and the interpretation of tidal signals. Ocean Dynamics 55, 124–136.

Pritchard, D., Hogg, A.J., 2003. Cross-shore sediment transport and the equilibrium morphology of mudflats under tidal currents. Journal of Geophysical Research 108 (C10), 11-1–1-15.

Pritchard, D., Hogg, A.J., Roberts, W., 2002. Morphological modeling of intertidal mudflats: the role of cross-shore tidal currents. Continental Shelf Research 22, 1887–1895.

Quaresma, V.S., Bastos, A.C., Amos, C.L., 2007. Sedimentary processes over an intertidal flat: a field investigation at Hythe flats, Southampton Water (UK). Marine Geology 241, 117–136.

Reed, D.J., 1990. The impact of sea-level rise on coastal salt marshes. Progress in Physical Geography 14, 465–481.

Ren, M., 1992. Human impact on coastal landform and sedimentation – the Yellow River example. GeoJournal 28, 443–448.

Ridderinkhof, H., 1997. The effect of tidal asymmetries on the net transport of sediments in the Ems Dollard Estuary. Journal of Coastal Research SI 25, 41–48.

Ridderinkhof, H., 1998. On the sensitivity of the large scale transport and distribution of fine-grained sediments in a tidal basin to the formulation of the erosion-sedimentation cycle. In: Dronkers, J., Scheffers, M.B.A.M. (Eds.), Physics of Estuaries and Coastal Seas. Balkema, Rotterdam, pp.145–153.

Ridderinkhof, H., van der Ham, R., van der Lee, W., 2000. Temporal variations in concentration and transport of suspended sediment in a channel-flat system in the Ems-Dollard estuary. Continental Shelf Research 20, 1479–1493.

Riethmüller, R., Heineke, M., Kühl, H., Keuker-Rüdiger, R., 2000. Chlorophyll a concentration as an index of sediment surface stabilisation by microphytobenthos? Continental Shelf Research 20, 1351–1372.

Roberts, W., Le Hir, P., Whitehouse, R.J.S., 2000. Investigation using simple mathematical models of the effect of tidal currents and waves on the profile shape of intertidal flats. Continental Shelf Research 20, 1079–1097.

Roberts, W., Whitehouse, R.J.S., 2001. Predicting the profile of intertidal mudflats formed by cross-shore tidal currents. In: McAnally, W.H., Mehta, A.J. (Eds.), Coastal and Estuarine Fine Sediment Transport: Processes and Applications. Elsevier, Amsterdam, pp. 263–285.

Schuttelaars, H.M., de Swart, H.E., 1999. Initial formation of channels and shoals in a short tidal embayment. Journal of Fluid Mechanics 286, 15–42.

Scully, M.E., Friedrichs, C.T., 2007. Sediment pumping by tidal asymmetry in a partially-mixed estuary. Journal of Geophysical Research 112, C07028. doi:10.1029/2006JC003784.

Tolhurst, T.J., Friend, P.L., Watts, C., Wakefield, R., Black, K.S., Paterson, D.M., 2006. The effects of rain on the erosion threshold of intertidal cohesive sediments. Aquatic Ecology 40, 533–541.

Van der Wegen, M., Wang, Z.B., Savenije, H.G., Roelvink, J.A., 2008. Long-term morphodynamic evolution and energy dissipation in a coastal plain, tidal embayment. Journal of Geophysical Research 113, F03001. doi:10.1029/2007JF000898.

Van Rijn, L.C., 1998. Principles of Coastal Morphology. Aqua Publications, Amsterdam, 730 pp.

Van Straaten, L.M.J.U., Kuenen, P.H., 1958. Accumulation of fine-grained sediments in the Dutch Wadden Sea. Geologie en Mijnbouw 19, 329–354.

Waeles, B., Le Hir, P., Silva Jacinto, R., 2004. Modélisation morphodynamique cross-shore d'un estan vaseux. Comptes Rendus Geoscience 336, 1025–1033.

Wells, J.T., Adams, C.E., Park, Y.A., Frankenberg, E.W., 1990. Morphology, sedimentology and tidal channel processes on a high-tide-range mudflat, west coast of South Korea. Marine Geology 95, 111–130.

Wells, J.T., Kemp, G.P., 1986. Interaction of surface waves and cohesive sediments: field observations and geologic significance. In: Mehta, A.J. (Ed.), Estuarine Cohesive Sediment Dynamics. Springer, New York, NY, pp. 43–65.

Widdows, J., Blauw, A., Heip, C.H.R., Herman, P.M.J., Lucas, C.H., Middelburg, J.J., Smchmidt, S., Brinsley, M.D., Twisk, F., Verbeek, H., 2004. Role of physical and biological processes in sediment dynamics on a tidal flat in Westerschelde Estuary, SW Netherlands. Marine Ecology Progress Series 274, 41–56.

Woodroffe, C.D., 2002. Coasts: Form, Process and Evolution. Cambridge University Press, Cambridge, 640 pp.

Wright, L.W., 1995. Morphodynamics of Inner Continental Shelves. CRC Press, Baco Raton, FL, 241 pp.

Yang, S.L., Friedrichs, C.T., Shi, Z., Ding, P.X., Zhu, J., Zhao, Q.Y., 2003. Morphological response of tidal marshes, flats and channels of the outer Yangtze River mouth to a major storm. Estuaries 26, 1416–1425.

Yang, S.L., Li, H., Ysebaert, T., Bouma, T.J., Zhang, W.X., Wang, Y.Y., Li, P., Li, M., Ding, P.X., 2008. Spatial and temporal variations in sediment grain size in tidal wetlands, Yangtze delta: on the role of physical and biotic controls. Estuarine Coastal and Shelf Science 77, 657–671.